ENHANCEMENT OF PHOTOCONVERSION EFFICIENCY OF P3HT:PCBM POLYMER SOLAR CELL USING SQUARYLIUM III DYE

By

Moses Tembo

A Dissertation submitted in partial fulfillment of the requirements for the award of the degree of Master of Science in Physics.

The University of Zambia

2016

DECLARATION

I, Moses Tembo, do hereby declare that this dissertation represents my own work and that it has not previously been submitted for the degree of Master of Science in Physics at this or any other University.

Author's signature:…….. Date: ……

NOTICE OF COPYRIGHT

CERTIFICATE OF APPROVAL

This dissertation by Moses Tembo has been approved as partial fulfilment of the requirements for the award of the degree of Master of Science in Physics at the University of Zambia.

EXAMINERS SIGNATURES

1…… Date:…….

2…… Date:……...

3:…… Date:……

DEDICATION

I dedicate this thesis to my elder brother Given Tembo and my daughter Roxana who have been very supportive and a great source of inspiration in my life.

ABSTRACT

Ternary systems comprising of poly(3-hexylthiophene)(P3HT):(6,6)-phenyl-C_{61} butyric acid methyl ester (PCBM) and varying amounts of squarylium dye III (SQ3) were prepared and deposited by spin coating to obtain nano-size thin films. The films produced were subsequently annealed at 140 °C for 10 min. Absorption spectra and electrical measurements were used to evaluate the effects of thermal annealing and dye loading on the different blends. The films were characterized for their surface morphology and film thickness using atomic force microscopy. Photo-conversion efficiencies were determined following current density – voltage (*J-V*) measurements under dark and illumination conditions enabling determination of various solar cell parameters. A significant increase in the maximum peak absorbance, from 0.30 to 0.35 a.u. was observed by incorporating SQ3 molecules at 13 % w/w loading. The absorption range was also observed to broaden (400 – 700 nm) extending to the near infra-red. The inclusion of SQ3 molecules resulted in enhanced light harvesting capacity due to widening of the absorption range. This consequentially resulted in an increase in photogenerated excitons and short circuit current (I_{sc}). The HOMO of SQ3 is reported to be located between the HOMO and LUMO of levels of P3HT and PCBM. It has been further suggested that incorporation of SQ3 molecules introduce a second exciton generation system and charge transfer mechanism. Photoinduced charge transfer is not only favourable between P3HT and PCBM but also between SQ3 and PCBM. Thus, the synergistic effect of improved light harvesting characteristics with additional exciton generation and charge transfer mechanism resulted in an increase in photoconversion efficiency (η). The open circuit voltage (V_{oc}), I_{sc}, fill factor (FF) and η in the control P3HT:PCBM were 0.53 V, 5.78 mA, 0.35 and 1.3 % which change to 0.64 V, 9.68 mA, 0.40 and 3.9 % in P3HT:SQ3:PCBM blends. Thus the inclusion of SQ3 into the P3HT:PCBM polymer blends resulted in a threefold increase in photoconversion efficiency.

ACKNOWLEDGEMENTS

First and foremost, I thank the almighty God for the wisdom, strength, knowledge and understanding he has granted me.

I am greatly indebted to my supervisors, Dr. M. O. Munyati, and Dr. S. Hatwaambo for their professional, careful and useful comments whilst preparing the research proposal and through all the stages of writing this dissertation. You have given me memories for life; I hope that I have given you something back. I will remember your incredible help and inspiring discussions.

I wish to express my gratitude to all those who helped with advice, encouragement and provision of materials that made it possible for me to compile and write this dissertation.

I am also grateful to the following for their various contributions Prof. Malik Maaza, Prof. Chris Arendse, Prof. Pan Kaloyerou, Prof. Prem C. Jain, Dr. H. V. Mweene, Dr. Rekha Rajan, Dr. Magret Samiji and Dr Nuru Mlyuka for providing useful information for the study.

My gratitude go to the Departments of Physics and Chemistry at the University of Zambia for the initial experiments, the Materials Research Group (MRG) of iThemba Labs of Cape Town in South Africa and the Physics Department of the University of Western Cape for the research facilities. I am thankful to the International Science Program (ISP) of Uppsala University in Sweden for sponsoring most of my MSc. degree program. I also thank the Department of Physics of the University of Dar-es-salaam and Material Science for East Central and Southern Africa (MSSEESA) for research facilities and financial support.

My heartfelt appreciation goes to my parents Mr. and Mrs. Tembo, my brothers Given, Soft and Abel and my sisters Esther, Rodah, Delphine and Deli for the support and encouragement they always offer me.

I also sincerely thank all my friends Mbawe, Kenan, Herryman, Adolph, Elias, Eliab, Joseph, Daniel, Dennis, Bonaventure, Boniface, Alex, Nelson, Natasha, Chileshe, Moses, Ganizani,

Jimmy, Isaiah, Kelvin, Noel and Martin for making my life memorable. Thank you for the support and encouragement in my academic life. May God bless!

Finally, thank you, Mirriam, love of my life and mother to my daughter. You never doubted that I could do this, even when I sometimes did. You make me stronger than I would be without you.

TABLE OF CONTENTS

LIST OF TABLES

LIST OF FIGURES

LIST OF ABBREVIATIONS

a.u	Arbitrary units
AFM	Atomic force microscope
Al	Aluminium
AM	Air mass
amu	Atomic mass units
A_{sc}	Area of solar cell
ASTM	American Society for Testing and Materials
BHJ	Bulk hetero-junction
C_6	Coumarin 6 dye
C_{60}	Buckminsterfullerene
D-A	Donor-acceptor
DAD	Donor-acceptor-donor
DSC	Dye sensitized
E	Radiative photon energy
E_g	Band-gap
eV	Electron volt
FF	Fill factor
h	Planck's constant = 6.63×10^{-34}J.s
H.E.P	Hydro-electric power
FRET	Förster resonance energy transfer
HOMO	Highest occupied molecular orbital
I	Current
I_m	Output current of the maximum electrical power
In_2O_3	Indium oxide

I_{sc}	Short circuit current
ITO	Indium tin oxide
J-V	Current-voltage
J_{max}	Maximum current
J_{sc}	Short circuit current density
k_B	Boltzmann's constant
LED	Light emitting diode
LUMO	Lowest unoccupied molecular orbital
$n(\omega)$	Number of photons
NADPH	Nicotinamide adenine dinucleotide phosphate
NIR	Near infrared
nm	Nanometer
OPV	Organic photovoltaic
P3HT	poly (3-hexylthiophene)
PCBM	(6, 6)-phenyl C_{60} butyric acid methyl ester
PCE	Power conversion efficiency
PEDOT:PSS	3, 4-polyethylenedioxythiophene-polystyrenesulfonate
PHJ	Planar hetero-junction
P_{inc}	Incident power
P_{max}	Maximum power point
P_{out}	Output power
PSC	Polymer solar cell
PV	Photovoltaic
q	Elementary charge = $1.60217662 \times 10^{-19}$ C
QE	Quantum efficiency

R_{rms}	Root mean square roughness
rpm	Revolutions per minute
SnO_2	Tin oxide
SQ3	Squarylium dye III
STP	Standard temperature and pressure
T	Kelvin temperature
T_g	Glass transition temperature
TiO_2	Titanium dioxide
UV	Ultraviolet
V	Voltage
Vis	Visible
V_{max}	Maximum output voltage
V_{oc}	Open circuit voltage
ZnO_2	Zinc oxide
γ	Zenith angle
η	Power conversion efficiency
π	Double bond or constant = 3.142
σ	Single bond
ω	Frequency
Ω	Ohms

CHAPTER 1

INTRODUCTION

This chapter gives an introduction to the dissertation by giving the motivation and describing purpose of the study.

1.1 MOTIVATION

Energy is essential to modern society and the global demand for it continues to grow every year. The worldwide consumption of energy has increased every year over the last 30 years [1, 2]. Global energy consumption grew by 2.4 % in 2007 and analysts predict a further 50 % increase from 2005 to 2030 [3-5]. The increase in energy consumption is attributed to the overall growth of world population and development in areas such as Africa and Asia [6]. The worldwide demand for energy is mostly supplied by fossil fuels and nuclear energy. However, these resources are limited and their use has negative environmental impacts [7]. Fossil fuels are burnt to release the chemical energy that is stored within this resource. This combustion of fossil fuel meets over 85 % of the energy demand of the world but is considered to be the largest contributing factor to the release of greenhouse gases into the atmosphere [8]. The other disadvantage of fossil fuel is that it is non-renewable and hence is a depleting resource. On the other hand, the use of nuclear power as an energy source is not accepted by a wide section of the population because of security and health risks. Furthermore, the disposal of nuclear waste is still an unsolved problem [9].

Hydro-electric power (H.E.P) is the main source of energy in urban areas of Zambia whilst most rural areas depend on diesel generators. H.E.P does not contribute significantly to greenhouse emission but its ability to penetrate rural areas of the country remains prohibitively expensive. This can be attributed to the high cost of rural electrification [10].

Solar energy has the potential to be an alternative source of electricity in rural communities while mitigating the factors leading to global warming.

Most conventional solar energy conversion devices are based on silicon technology. However, fabrication of silicon based solar cells is expensive because it requires a very clean environment. The silicon solar cells tend to be heavy and not flexible. Thus, silicon based solar cells tend to be beyond the financial reach of most people [11]. Solution-processed organic solar cells are therefore being developed to replace silicon solar cells [12]. Nanostructured polymer solar cells (PSC) have also evolved as another potential alternative [13]. The fabrication of PSCs by processing polymers from solution and printing them onto different types of substrates by roll-to-roll production processes like newspapers offers important advantages over their inorganic counterparts due to low cost of fabrication and easy processing of the photoactive layer [14-16]. PSCs are lightweight, mechanically flexible, and the properties of the photoactive layer can be tuned by adjusting the chemical architecture of its components.

The need to look for renewable energy sources to replace the fossil fuels has driven substantial research effort into the energy sector [17]. The Sun's energy is the primary source of most forms of energy found on earth. Solar energy is clean, abundant and renewable. It has the potential to benefit the world by diversifying the energy supply and reducing dependence on fossil fuels [18]. Solar electricity has steadily grown in importance as an energy technology, with solar cells finding use in a variety of applications ranging from spacecraft to small portable devises [19].

1.2 STATEMENT OF THE PROBLEM

Most commercial solar cells are currently made from refined, highly purified silicon crystals. However, the high cost of silicon solar cells and their complex production process have caused

interest in alternative photovoltaic technologies. As an example, polymer solar cells offer the possibility of large area, ultra-thin, flexible and low-cost devices, which can be fabricated with organic polymers at low temperature and employing well established processing techniques, such as spin-coating, screen-printing, spray-coating and ink-jet printing. However, the low quantum efficiency and low power conversion efficiency (η) of polymer solar cells has inhibited their development. Whereas the open circuit voltage (V_{oc}) and the fill-factor (FF) of polymer solar cells are in the range of inorganic solar cells, the short circuit current (I_{sc}) is nearly a factor ten lower. The low I_{sc} results in low charge collection and subsequently low power conversion efficiency. This low I_{sc} is mainly caused by the mismatch between the optical absorption of the organic polymers and the solar spectrum. This problem is addressed by incorporating an organic dye, namely squarylium dye III (SQ3) molecules, into the poly (3-hexylthiophene) (P3HT) and a fullerene derivative (6, 6) phenyl-C_{61}-butyric acid methyl ester (PCBM) solar cell photoactive layer to increase light absorption of the systems**.** It is anticipated that more efficient polymer solar cells will lead to lower cost PSC, resulting in rapid penetration of the technology and the provision of electricity to remote areas.

1.3 AIM

To study optimization factors for power conversion efficiency of polymer:fullerene solar cells based on P3HT:PCBM blend by incorporating SQ3 molecules.

1.4 SPECIFIC OBJECTIVES

(i) To compare the spectral absorbance of the P3HT:SQ3:PCBM thin films produced at different annealing temperatures and having different film thicknesses.

(ii) To determine the optimum dye content for optimum photo-absorption in the P3HT:SQ3:PCBM blend thin films.

(iii) To evaluate the surface morphology and film thickness of the prepared P3HT:SQ3:PCBM thin films.

(iv) To optimize the morphology of the prepared P3HT:SQ3:PCBM thin films.

(v) To investigate the effect of annealing temperature and film thickness on the spectral characteristics of P3HT:SQ3:PCBM blends.

(vi) To determine the power conversion efficiency of the fabricated PSC.

1.5 HYPOTHESIS

The efficiency of PSCs can be enhanced by enlarging the absorption spectrum to include the near infrared region of the absorption spectrum. It is anticipated that the incorporation of SQ3 molecules into the P3HT:PCBM active layer will increase absorption by including the near infra-red region of the absorption spectrum. This will increase the number of photons absorbed by the solar cell active layer. It is further anticipated that annealing will optimize the material's morphology by narrowing the band-gap and widening the absorption spectrum. The optimized morphology helps increase the efficiency of solar cells by facilitating both the photo induced creation of mobile charge carriers as well as the transport of the carriers to the electrodes.

1.6 SIGNIFICANCE OF THE STUDY

The technology of photovoltaic systems based on inorganic semiconductor materials has matured over the years. These systems have high manufacturing costs and are characterized by a lack of flexibility. The former makes them unaffordable for large scale applications to many people while the latter limits their acceptance. PSCs on the other hand offer the possibility of low-cost mass production as well as flexibility in applications. The key to commercial realization of the polymer based photovoltaic technologies is increasing their efficiency to match those of traditional silicon based systems. This study anticipates the enhancement of the power conversion efficiency of P3HT:PCBM films by fine tuning of the morphology and the increase of photo absorption through dye sensitization. This is the first time SQ3 molecules are

incorporated into the P3HT:PCBM photoactive layer. The body of knowledge generated will contribute towards accelerating the commercialization of organic solar cells.

1.7 THESIS/RESEARCH QUESTIONS

The research answers the following questions:

(1) How can we increase the absorption efficiency, which is low for large band-gap organic materials?

(2) How can we enlarge the absorption spectrum of PSCs to include even the near-infrared region of the solar spectrum?

(3) How can we facilitate successful dissociation of excitons upon light absorption in organic semiconductors and overcome recombination during the transportation of the charges to electrodes?

(4) How can we optimize exciton separation and the light harvesting capacity of the thin film cells?

(5) How can we increase the low power-conversion efficiency of PSCs?

1.8 AIR MASS AND SOLAR SPECTRUM

The air mass (AM) is the path length which light takes through the atmosphere normalized to the shortest possible path length (when the Sun is directly overhead). The AM quantifies the reduction in the power of light as it passes through the atmosphere and is absorbed by air and dust.

The AM is used to characterize the performance of the solar cell under standardized conditions. The AM is given by equation (1).

$$AM = \frac{actual\ optical\ path}{diameter\ of\ the\ atmosper} = cosec\ (\gamma) \quad (1)$$

Where γ is the zenith angle.

A solar reference cell is simply a small area (2 cm x 2 cm) solar cell packaged in a metal housing under a glass window intended for use indoors to set simulated sunlight levels. The extra-terrestrial spectrum of the sun resembles that of a black body with temperature given by the temperature on the surface of the Sun. The Standard Testing Conditions (STCs) of solar cells are as follows:

i. temperature of the device under test must be 25 ± 1 °C,
ii. spectral distribution of the light must be AM 1.5 ± 25 % and
iii. irradiance measured at the plane of the solar cell must be 1 Sun (100 mW/cm^2) ± 2 %.

The spectral distribution of the solar radiation (the number of photons of a particular energy as a function of frequency) is given by equation (2).

$$n(\omega) = \left(\frac{2\pi h}{c^2}\right) \frac{\omega^3}{\exp\left(\frac{E}{k_B T}\right) - 1} \quad (2)$$

Where $n(\omega)$ is the number of photons, ω is the frequency, k_B is the Boltzmann constant, c is the speed of light, h is the Planck constant, T is the surface temperature of the Sun and E is the radiative photon energy given by Planck's equation (3)

$$E = \frac{h}{2\pi}\omega \quad (3)$$

Here, h is Planck's constant = 6.63x10^{-34} J.s and ω is the frequency.

The efficiency of a solar cell is sensitive to variations in both the power density and the spectrum of the incident light. The solar spectrum changes throughout the day and with location. Standard reference spectra are defined to allow the performance comparison of photovoltaic devices from different manufacturers and research laboratories. The two solar cell standard spectra are shown in Figure 1.

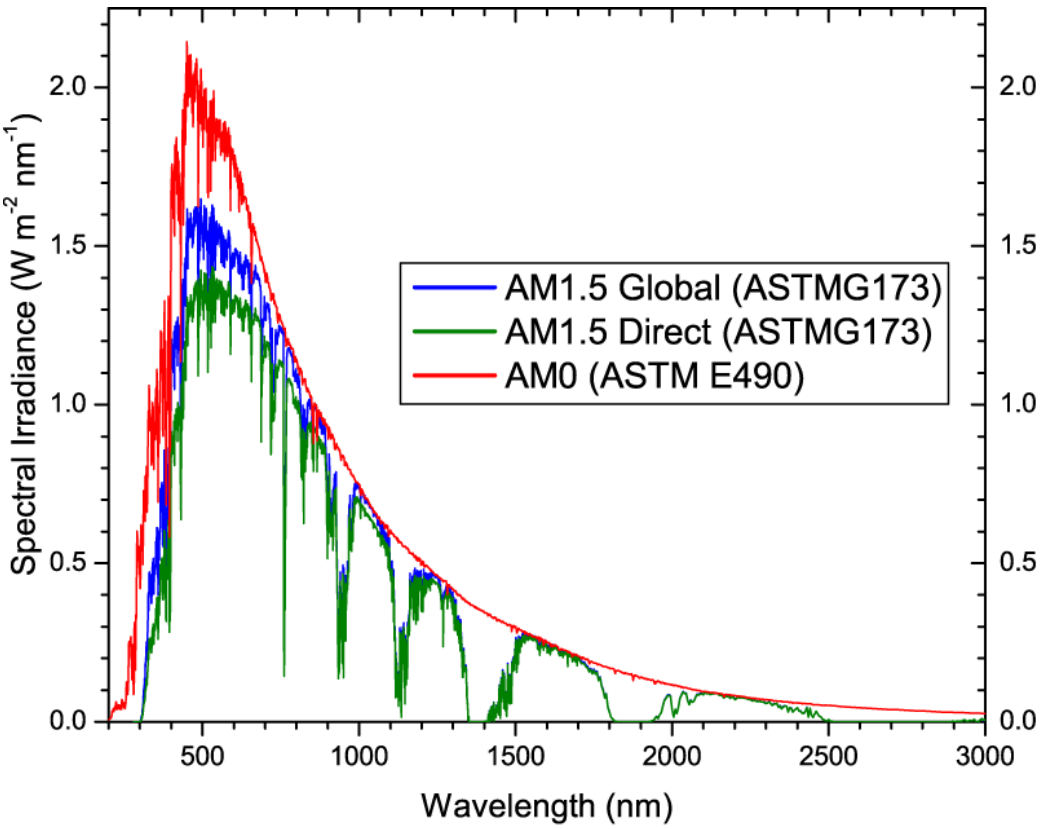

Figure 1: Standard solar spectra [20]

The standard spectrum outside the earth's atmosphere is called AM 0, because at no stage does the light pass through the atmosphere. This spectrum is typically used to predict the expected performance of cells in space. The AM 1.5 Global (AM 1.5 G) is the standard spectrum at the earth's surface and includes both direct and diffuse radiation. The intensity of AM 1.5 Direct (AM 1.5 D) radiation can be approximated by reducing the AM 0 spectrum by 28 %. The global spectrum is 10 % higher than the direct spectrum. These calculations give approximately 970 W/m^2 for AM 1.5 G. However, the standard AM 1.5 G spectrum has been normalized to give

1000 W/m^2 (100 mW/cm^2) due to the convenience of the round number and the fact that there are inherently variations in incident solar radiation.

CHAPTER 2

THEORETICAL BACKGROUND AND LITERATURE REVIEW

This chapter presents the theoretical background of polymer solar cells and the literature review.

2.1 THEORETICAL BACKGROUND OF PSC

The operational physics of PSCs provides the foundation for device improvement through molecular design. In a typical PSC, light absorption creates strongly bound excitons (electron-hole pairs) [21]. The strongly bound excitons exist because of the low dielectric constants in the organic components, which are insufficient to affect direct electron-hole dissociation as is found in the high dielectric inorganic counterparts [22, 23]. In PSCs, exciton dissociation occurs almost exclusively at the interface between two materials of differing electrons affinities and ionization potentials (the electron donor and the electron acceptor). The selection of an appropriate donor-acceptor (D-A) pair and good device architecture is important if an effective photocurrent is to be generated. PSCs have a planar-layered structure in which the organic light absorbing layer is sandwiched between two different electrodes.

In PSCs the conversion of the incident solar radiation to an electric current is essentially through the following step:

(i) the absorption of the incident photons,

(ii) the generation of the excitons,

(iii) the dissociation of excitons into free charge carriers,

(iv) the transport of free charges and

(v) charge collection at the electrodes.

All the five mentioned steps are potential targets for researchers seeking to improve the performances of the PSCs. When light is absorbed in a PSC, an electron is promoted from the highest occupied molecular orbital (HOMO) to the lowest unoccupied molecular orbital (LUMO), forming an exciton. Absorption efficiency mainly depends upon the absorption spectra of the organic materials used. However, the design of the devices, such as the photoactive layer film thickness also has a role to play in the capture process. The dissociation of excitons into free charges depends on the properties of the donor and the acceptor. The asymmetrical ionization energy and difference in work function of the electrodes creates an electric field. This asymmetry is the reason why electron flow is more favoured in the direction from the lower work-function electrode to the higher work-function electrode (forward bias). The fourth step is the transport of the free charges through the sample and their collection at the electrodes. The electrons must reach one electrode while the holes must reach the other electrode. The final step is crucial because organic film structures are generally amorphous and disordered and consequently charge recombination is strongly favoured.

PSCs convert light directly into electricity without the costs associated with the generation of electric power. Furthermore, PSCs require little maintenance and are reliable because they have no moving parts. PSCs are environmentally friendly, renewable and they contribute to the reduction of the carbon dioxide emission associated with fossil fuels and biomass. PSCs have a high potential of dominating the energy market due to their low production cost, flexibility and light weight [25]. The photoactive layer of PSCs can be processed from solution in a single step by using simple techniques such as spin-coating and screen-printing [26].

The state of art in PSCs is currently represented by BHJ solar cells which are based on poly (3-hexylthiophene) (P3HT) and the fullerene derivative (6,6)-phenyl-C_{61}-butyric acid methyl

ester (PCBM) with reproducible efficiencies approaching 5% [27]. An understanding of the electronic interactions between the polymeric donors and the fullerene acceptors as well as the complex interplay of device architecture and morphology is necessary to attain high efficient PSCs. Two main approaches have been explored in an effort to develop viable PSC devices. These are the bulk hetero-junction (BHJ) and the planar hetero-junction (PHJ) as shown in Figure 2.

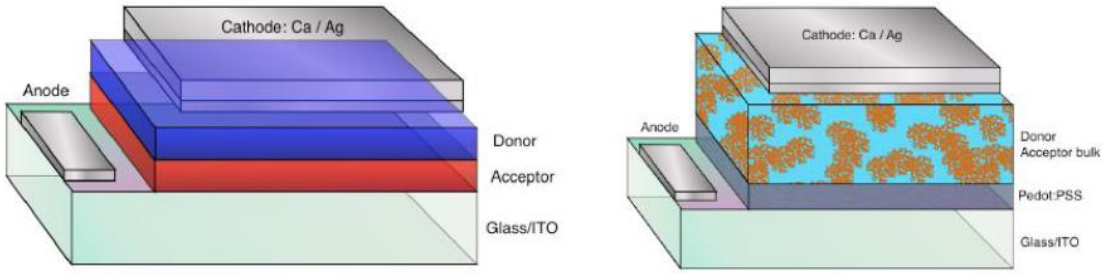

Figure 2: Schematic diagrams of PHJ (left) and BHJ (right) PSCs [28]

In PHJ, two organic materials are deposited one on top of the other. The disadvantage of PHJ devices is that the active layer is limited by the exciton diffusion length which is less than 20 nm. Consequently, only the excitons formed within a narrow region adjacent to the donor/acceptor interface can be separated into free charge carriers.

The BHJ is where the donor and acceptor materials are intimately blended throughout the bulk [29–32]. In this way, excitons do not need to travel long distances to reach the donor acceptor interface and charge separation can take place throughout the whole depth of the active layer. Thus every absorbed photon in the photoactive layer can potentially contribute to the photocurrent. The basic operating principle of a BHJ device relies on the characteristics of phase-separated structures in the photoactive layer consisting of electron donors and acceptor components. The light incident upon the BHJ photoactive layer where the donor and the

acceptor components are segregated into phase-separated domains gives rise to the formation of excitons that must diffuse to the DA interface, where the electron–hole charge dissociation occurs [33]. The dissociated electrons and holes move through the percolated domains toward their corresponding electrodes, ultimately accomplishing the power conversion from solar energy into electric energy [34]. The morphology of the photoactive layer is a critical factor to be optimized for BHJ device performance [35, 36]. The thickness of the photoactive layer is also an important factor in the absorption of light and thus exciton generation inside the layer [37-39]. The fundamental physical processes in a BHJ device are schematically represented in an energetic diagram as depicted in Figure 3.

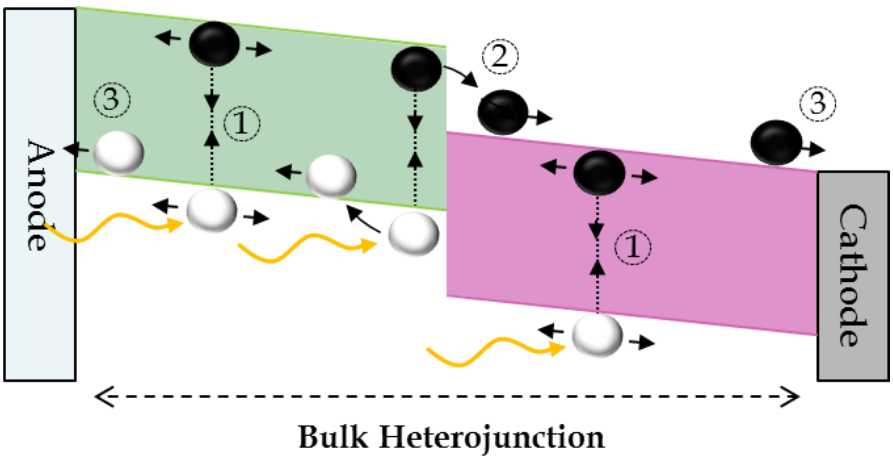

Figure 3: The working principle of BHJ PSC

Light enters the cell through the transparent anode and is absorbed in the BHJ layer. This is followed by excitons generation (1). The excitons diffuse in the BHJ until they either recombine or reach a donor-acceptor interface (2), where they separate into electrons (black) and holes (white). The electrons and holes will then move to the respective anode and cathode, through the donor and acceptor material phase (3).

2.2 GENERAL PARAMETERS OF A SOLAR CELL

The electrical performance of a polymer solar cell is characterized by short-circuit current density (J_{sc}) often simply noted as short circuit current (I_{sc}), open-circuit voltage (V_{oc}) and fill-factor (*FF*). The open circuit voltage, the short circuit current and the maximum power point are derived from the plotted current density–voltage *(J-V)* curve as shown in Figure 4.

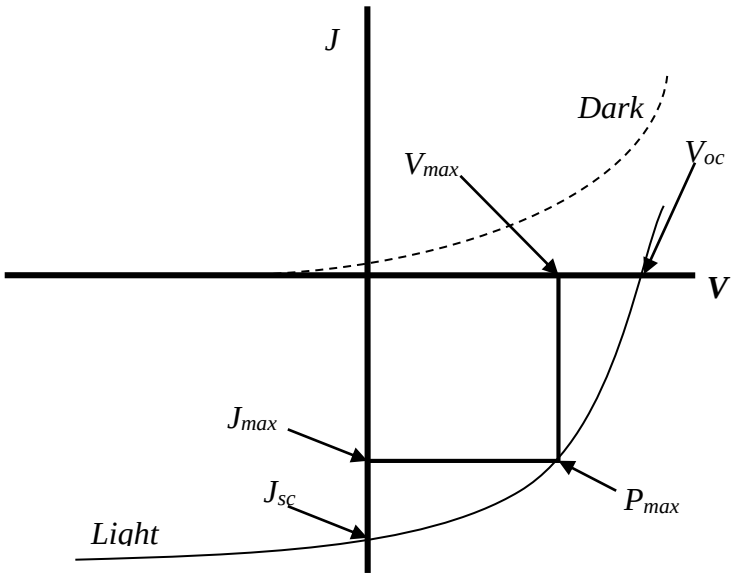

Figure 4: The typical current density–voltage (*J-V*) characteristics of a PSC

2.2.1 Open circuit voltage (V_{oc})

Open circuit voltage is the maximum possible voltage across a photovoltaic cell. This is the voltage across the cell in sunlight when no current is flowing. Open circuit voltage is mostly determined by the electronic structure of the photovoltaic device. The difference between the lowest unoccupied molecular orbital (LUMO) of acceptors and the highest occupied molecular orbital (HOMO) of donor is the main reason for the open circuit voltage. The value of the open circuit voltage for a PSC is expressed by the empirical equation (4).

$$V_{oc} = \frac{|E_{HOMO\ donor}| - |E_{LUMO\ acceptor}|}{q} - 0.3\ eV \quad (4)$$

Here q is the elementary charge =1.60217662x10^{-19} C and 0.3 eV is the result from the temperature dependence of the quasi-Fermi-levels in the polymer and fullerene domains a conclusion based upon the fundamental statistics of fermions.

2.2.2 Short circuit current density (J_{sc})

An illuminated solar cell can take the place of a battery or a current generator in a simple electric circuit. The short circuit current (I_{sc}) is the current through the cell when the voltage across the solar cell is zero. The I_{sc} is given by equation (5).

$$I_{sc} = \int QE(E)n(\omega)dE \quad (5)$$

Here QE is the quantum efficiency and $n(\omega)$ is the solar flux of photons with energy E given by Planck's equation. QE is a material constant and is defined as the probability for an incident photon to generate an electron at the external circuit. Generally, QE depends on the absorption coefficient, the efficiency of charge separation and the efficiency of charge collection. Since the I_{sc} is roughly proportional to the area of the solar cell, the short circuit current density (J_{sc} = I_{sc}/A) is often used for solar cell characterization.

2.2.3 Maximum power point (P_{max})

Power (P) is the product of current and voltage. The maximum power point is the point on the *J–V* curve where the area of the resulting rectangle is largest. The maximum power point is the product of maximum current density (J_{max}) and maximum voltage (V_{max}):

$$P_{max} = J_{max}V_{max} \quad (6)$$

2.2.4 Fill factor (*FF*)

Fill factor (*FF*) is another important parameter that needs to be optimized to obtain a highly efficient solar cell. *FF* is a measure of the square-ness of the current-voltage curve of a solar

cell under light. *FF* is the ratio of a photovoltaic cell's actual maximum power output to its theoretical power output if both current and voltage are at their maxima as given by equation (7).

$$FF = \frac{J_{max}V_{max}}{J_{sc}V_{oc}} \tag{7}$$

2.2.5 Power conversion efficiency *(η)*

PCE measures the amount of power produced by a solar cell relative to the power available in the incident solar radiation (P_{inc}). Incident solar radiation in this case is the sum over all wavelengths and is taken to be 100 mW/cm^2 when solar simulators are used. The power conversion efficiency (η) of a PSC is defined as the ratio of maximum power (P_{max}) to the incident power which is converted to electricity. The power conversion efficiency (η) is given by equation (8).

$$\eta = \frac{P_{max}}{P_{inc}} \tag{8}$$

Substituting equations (6) and (7) into equation (8) gives

$$\eta = \frac{P_{max}}{P_{inc}} = \frac{J_{max}V_{max}}{P_{inc}} = FF\frac{J_{sc}V_{oc}}{P_{inc}} \tag{9}$$

Thus, the device power conversion efficiency (η) can be enhanced by implementing fabrication procedures that increase J_{sc}, V_{oc} and *FF*.

2.3 THE MATERIALS OF THE PSCs

2.3.1 Regio-regular poly(3-hexylthiophene) (rr-P3HT)

Rr-P3HT is the most extensively studied conducting polymer. This is not only due to its ease of processing from solution and the fact that it is widely available but also due to its highly crystalline microstructure that gives rise to its promising electrical properties. It has been

shown that a systematic improvement in charge carrier mobility can be obtained by maximizing the regioregularity and the molecular weight of the polymer. The effect of increased regioregularity is to avoid out-of-plane twists along the backbone of the polymer, as monomers in a head to head orientation experience steric repulsions between adjacent alkyl groups. This disrupts the planarity of the molecule, decreasing the effective conjugation length of the polymer, as can be seen in the hypsochromatic shifts in optical absorbance as the region-regularity decreases [40]. This in turn reduces the efficiency of charge hopping. P3HT with a head to tail region-regularity in excess of 96 % has been shown to exhibit charge carrier mobility of up to 0.1 cm^2/Vs under inert atmospheric conditions [41].

The HOMO energy level of P3HT is 4.6 eV from the vacuum energy level as a consequence of the electron-rich, π-conjugated, highly planar aromatic backbone that has electron-donating alkyl side chains. P3HT self-organizes into a microcrystalline structure and because of efficient inter-chain transport of charge carriers, the hole mobility in P3HT goes up to approximately 0.1 cm^2/Vs. Moreover, in thin films, inter-chain interactions cause a red shift of the optical absorption of P3HT, which provides an improved overlap with the solar emission [42].

2.3.2 (6,6)-phenyl C_{60} butyric acid methyl ester (PCBM)

PCBM is extensively used as the electron accepting component in polymer solar cells. PCBM is a C_{60} fullerene derivative with an electron mobility of $2x10^{-3}$ cm^2/Vs. The LUMO of PCBM, which is a critical parameter for electron transfer, varies in range from 3.7 eV to 4.3 eV. The C_{60} molecule HOMO-LUMO optical gap is reported to be 1.9 eV [43].

The chemical structure of P3HT and PCBM is shown in Figure 5.

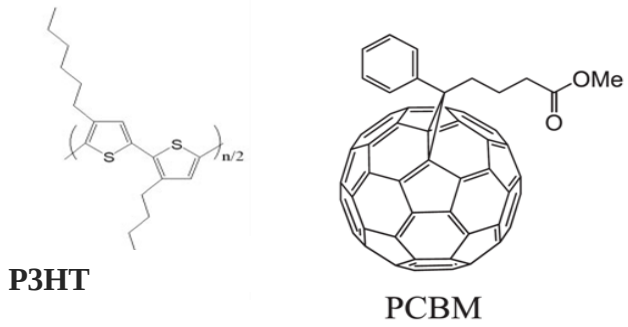

P3HT PCBM

Figure 5: Chemical structure of P3HT and PCBM [43].

2.3.3 3, 4-polyethylenedioxythiophene-polystyrenesulfonate (PEDOT:PSS)

PEDOT:PSS is a polymer mixture of two ionomers; a poly-edot called poly-ethylene-dioxythiophene (PEDOT) and sulfonated polystyrene known as poly(styrenesulfonate) (PSS). PEDOT carries positive charges while PSS carries negative charge. Together, the charged molecules form a macromolecular salt that is dissolved in polar solvents (usually water). The molecular structure of PEDOTPSS is shown in Figure 6. This conductive polymer has many properties that are useful if applied in organic solar cells. Firstly, a PEDOT:PSS thin film is a good hole transporting layer. PEDOT:PSS has work function between 4.9 eV and 5.2 eV that matches the HOMO level of P3HT. PEDOT has excellent transmission in the visible light region, good electrical conductivity of about 300 S/cm and is environmentally stable. A water dispersion of PEDOT doped with PSS is commercially available from many suppliers under the trade name of Baytron P. It has been observed that the deposition of a thin layer of PEDOT:PSS on an ITO surface increases the power conversion efficiency of many organic devices and also increases the lifetime of these devices. Furthermore, the PEDOT:PSS layer acts as a physical barrier against the many defect sites known to be present in the ITO thin films [44].

PEDOT:PSS improves the quality of the ITO electrode and aid hole (positive charge carrier) extraction from the active film. Figure 6 shows the chemical structure of PEDOT:PSS.

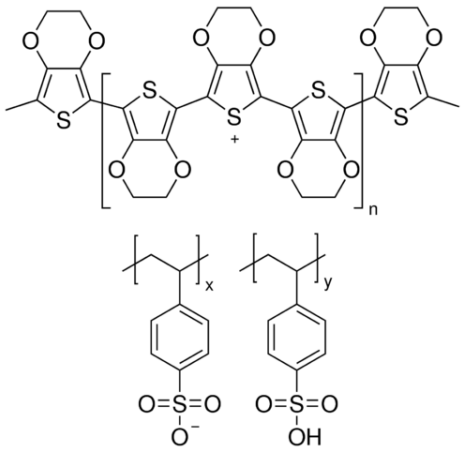

Figure 6: Molecular structure of PEDOT:PSS [45].

2.3.4 Squarylium dye III (SQ3)

SQ3 is an organic dye with molecular formula $C_{20}H_{20}N_2O_2$. The chemical structure of SQ3 is shown in Figure 7. SQ3 belongs to guaiazulenyl-derived squaraine dyes. The band gap of SQ3 is approximately 1.7 eV, with HOMO approximately 5.3 eV [46]. The chemistry of squaraines is well investigated and has been documented by Sreejith, Carol, Chithra and Ajayaghosh [47]. Squaraines are the main product of the condensation of electron-rich aromatics with squaric acid, a reaction that obeys the rules of aromatic electrophilic substitution. The efficient synthesis of squaraines relies on an optimal electron richness of the aromatic substrate and on the capability of the latter to stabilize partial positive charge. squaraines belong to the class of polymethyne dyes with resonance-stabilized zwitterionic (an ion with both a positive and negative charge) structures. They are structurally flat, highly conjugated organic molecules, which are expected to stack very closely in crystals and allow for fast charge transport through overlapping p-orbitals. Squaraine molecules typically consist of an electron deficient central four-membered ring and two electron-donating groups in a donor–acceptor–donor (DAD)

formation. This configuration enables the transport of holes via the acceptor, and electrons via the donor groups. The squaraines are known to absorb over the whole visible and near infrared spectrum due to the small band-gap energy which is approximately 1.2 eV. This makes them particularly interesting for photovoltaic and light-sensing applications. The narrow band-gap of squaraines is also expected to facilitate ambipolar injection from a single electrode material with suitable work function [48, 49]. Figure 7 shows the molecular structure of SQ3.

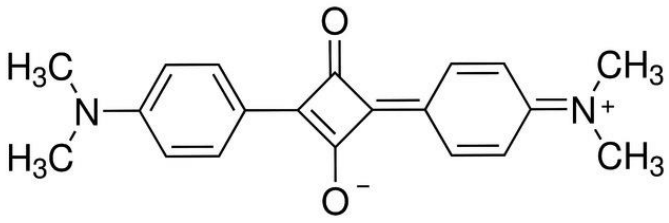

Figure 7: Molecular structure of SQ3 [50].

2.3.5 Indium Tin Oxide (ITO)

ITO is a transparent conductive material. It is a mixture of indium oxide (In_2O_3) and tin oxide (SnO_2) typically in the ratio of 9:1 respectively. ITO is used as the anode in the PSCs because of its electrical conductivity and optical transparency. ITO thin films have low resistivity due to the large free carrier density, which is in the range of 10^{20} /cm^3 to 10^{21} /cm^3. Thin films of ITO can be deposited on flexible substrates such as metal foils and polymers by electron beam evaporation, sputtering or spin processes at both low and high substrate temperatures. The work function of ITO is between 4.4 eV and 5.14 eV [51].

2.3.6 Aluminium (*Al*)

Aluminium is used in PSCs because it is lightweight, corrosion resistant, and easy to install. Aluminium is a good conductor of heat and electricity, has high reflectivity and is fully recyclable [52].

2.4 LITERATURE REVIEW

The first publication on the photovoltaic effect is attributed to the French scientist Becquerel [53-55]. In 1839, Becquerel measured a small electric current through a liquid when illuminating one of the two platinum rods immersed in it. Bell Laboratories scientists Chapin, Fuller and Pearson in 1954 developed a silicon photovoltaic cell and this led to the first commercial application of photovoltaic solar cells [56]. However, due to the high production cost, the main market for solar cells was for space applications and for power satellites. Much progress was made in the following 25 years. At present laboratory efficiency of over 24 % for mono-crystalline and over 19 % for multi-crystalline bulk silicone cells has been reported [57]. However, this conversion efficiency is reduced when industrial processing is involved. Putting several cells in a series connection to fabricate modules also lowers the overall efficiency.

The interplay of production cost and achieved energy conversion efficiency determines the overall cost of electricity produced by photovoltaic systems. This has led to a new type of photovoltaic solar cells based on organic materials incorporated in the active layer of the PV cell. Organic PVs focus on low cost solar cell devices. The high absorption coefficient of organic materials yields low thin films below one micrometre (1 μm) in thickness which can strongly reduce material cost. This has led to mechanical flexibility and very light devices. Organic materials have high potential for chemical modification and are thus suitable for low cost processing using solution based techniques such as spine coating and screen printing. By 1950, small conjugated molecules like anthracene were already being used for light emitting diode (LED) fabrication [58]. However, the requirement of high operating voltage of over

400V was prohibiting large commercial interest. This problem was addressed by Tang, Slyke and Chen who introduced a bi-layer hetero-junction of conjugated small molecules sandwiched between appropriate charge injecting contacts and this reduced the operating voltage to 10 V [59]. The first organic solar cells were based on an active layer made of a single material sandwiched between two electrodes of different work functions. The single layer organic solar cells had power conversion efficiencies of far below 1 % for the solar spectrum [60]. In 1977 Shirakawa, MacDiarmid and Heeger reported that polymer polyacetelene could be made highly conductive upon oxidation with chlorine, bromide or iodine vapour [61, 62]. Thereafter, new organic conjugated polymers such as polyaniline and PEDOT that can be made highly conductive were developed [63-65]. Another realization was the synthesis in the mid 1980's of macromolecule buckministerfullerene (C_{60}) as a new allotrope of carbon besides diamond and graphite [66, 67]. Small conjugated polymers like polythiophene have since the late 1980s been extensively studied [68, 69].

The field of organic PV was triggered in 1992 when it was discovered that ultrafast photo-induced electron transfer occurs from conjugated polymer to buckminsterfullerene (C_{60}) [70]. A major breakthrough in solar cell performance came in 1986 when Tang discovered that efficiencies of about 1 % can be attained when an electron donor (D) and electron acceptor (A) are brought together in one cell [71]. This donor–acceptor (DA) hetero-junction concept is at the heart of all three types of organic photovoltaic (OPV) cells that currently exist: dye-sensitized solar cells, planar organic semiconductor cells and bulk hetero-junction (BHJ) cells [72-76]. BHJ solar cells based on P3HT (which forms the hole-transport network) and PCBM (which forms the electron-transport network) are the most important investigations and studies are under way for improving their power conversion efficiency [77]. These devices offer considerable promise for use in new solar energy technologies due to their flexible material properties and the potential for low-cost manufacture [78]. The reported efficiencies for organic

solar cells have risen sharply, from the rather modest 1 % in the first BHJ device in 1995 to about 5 % in 2010 [79].

The dye sensitized solar cell (DSC) was originally co-invented in 1988 by O'Regan and Grätzel at the Ecole Polytechnique Federale de Lausanne [80]. Incorporation of dye molecules in some wide band-gap semiconductor electrodes was a key factor in developing the DSC. In the DSC, charge separation is accomplished by kinetic competition like in photosynthesis leading to photovoltaic action. It has been shown that DSC is promising class of low cost and moderate efficiency solar cell based on organic materials [81]. In fact, in semiconductor p-n junction solar cells, charge separation is taken care by the junction built in electric field, while in DSCs charge separation is by kinetic competition as in photosynthesis [82]. The organic dye monolayer in the photo-electrochemical or DSC replaces light absorbing pigments (chlorophylls), the wide band-gap nanostructured semiconductor layer replaces oxidized dihydro-nicotinamide-adenine-dinucleotide phosphate (NADPH), and carbon dioxide acts as the electron acceptor. Moreover, the electrolyte replaces the water while oxygen acts as the electron donor and oxidation product [83]. The overall cell efficiency of the DSC is found to be proportional to the electron injection efficiency in the wide band-gap nanostructured semiconductors. This finding has encouraged researchers over the past decade. Therefore, ZnO_2 nanowires have been developed to replace both porous and TiO_2 nanoparticle based solar cells [84]. Also, metal complex and novel man made sensitizers have been proposed [85]. However, processing and synthesization of these sensitizers are complicated and costly processes [86]. Development or extraction of photosensitizers with absorption range extended to the near infrared is greatly desired. Natural dye extracts provide non-toxic and low cost dye sources with high absorbance level of ultraviolet (UV), visible (Vis) and near infrared (NIR). Examples of such dye sources are Bahraini Henna and Bahraini raspberries [87]. SQ3 is an organic dye characterized by an aromatic four-membered ring system derived from squaric

acid. The squarylium dyes have been used as near-infrared absorbers and photoconductive materials in DSC.

In 2003, P3HT:PCBM cells with 3.5 % efficiency were reported, and in 2007 multiple groups reported efficiencies of 4.5 % with this material combination [88]. One of the reasons for decreasing organic solar cells efficiency in comparison with their inorganic counterparts is that the spectral range of the optical absorption of the conducting polymers is relatively narrow compared to the solar spectrum, where the limitation in light absorption across the solar spectrum limits the photocurrent of the solar cells [89]. In 2010, Ismail, Soga and Jimbo studied the effect of addition of a dye molecule in light harvesting and photocurrent of P3HT:PCBM solar cells [90]. They studied the effect of Coumarin 6 (C6) dye on light harvesting and photocurrent of the P3HT:PCBM solar cell. They found that the contribution of the C6 dye in light harvesting of the P3HT:PCBM solar cell occurs by increasing the dye concentration in the blends under the effect of thermal annealing at 140 °C. The absorption of the C6 increased with increasing its concentration in the blend.

Morphology optimization and improving the electrical interfaces have been shown to be crucial for PSC device efficiencies. Intensive engineering and improvement of the contacts has pushed up the power efficiency over 3 % [91]. Morphology manipulation of the photoactive layer is thus a key point for improving the device performance of polymer solar cells [92-94]. The nanoscale morphology of P3HT:PCBM is influenced by the spin casting solvent, the ratio of P3HT to PCBM and the solution concentration. The choice of solvent is important for obtaining good morphology of thin films as well as for efficiency and stability of the photovoltaic device [95]. Several solvents such as xylene, toluene, chloroform, chlorobenzene and 1, 2 dichlorobenzene have already been investigated in this respect. The thin films should be free from pinholes, kinks and overlapping chains. Thermal annealing is a possible approach to

enhancing the photon absorbance, improving the short circuit current and the fill factor. Optimizing the annealing temperature of the P3HT:PCBM film will also enhance the power conversion efficiency. During annealing, crystal growth and crystal perfection of both components occur, which increases charge transport capability. However, annealing at temperatures higher than 160 °C forces aggregation of both P3HT and PCBM. This results in large scale phase separation in the composite film [96]. Thus, accurate control of the annealing temperature is essential in order to gain high performance devices.

CHAPTER 3

EXPERIMENTAL METHOD

This chapter explains the different experiments that were carried out in the research. It also outlines the procedures carried out for morphological and electrical characterization of thin films.

3.1 POLYMER SOLAR CELL FABRICATION

In the present work, PEDOT:PSS was spin-coated as a buffer layer on the pre-cleaned ITO glass substrates and then annealed at 150 °C for 10 minutes. Then the active layer (P3HT:SQ3:PCBM) was spin-coated on top of the PEDOT:PSS layer. Finally, an Al layer with a thickness of about 80 nm was deposited by using evaporation beam. The PSC device structure is shown in Figure 8. It consisted of glass coated ITO as the top electrode, photoactive layer consisting of P3HT:SQ3:PCBM and an *Al* bottom electrode.

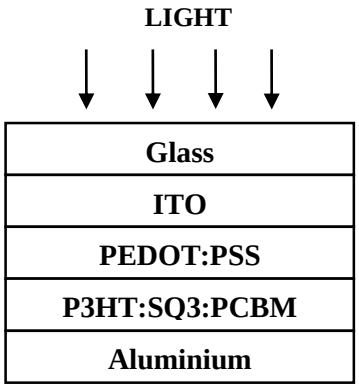

Figure 8: The device structure of polymer solar cell.

The specific method used to deposit each of the materials is described in the following sections:

3.1.1 Conditioning and cleaning of ITO coated glass

ITO coated on a 25 mm x 35 mm x 1.1 mm glass substrate with a sheet resistance between 10 Ohms/square (Ω/□) and 15 Ω/□ was purchased from Hallo Chemicals Pharmaceutical Import and Export Limited. The ITO coated glass substrates were cut into pieces of 1 cm^2 size and cleaned by an Ultrasonic Cleaner. The ITO substrate was cleaned sequentially in methanol, acetone, trichloroethylene, acetone, ethanol and de-ionized water. The cleaned ITO coated glass was dried using a stream of gaseous nitrogen.

3.1.2 PEDOT:PSS deposition

The PEDOT:PSS thin film was deposited using the spin coating technique. Spin coating is a procedure used to apply uniform thin films to flat substrates. An excess amount of solvent is placed on the substrate, which is rotated at high speed in order to spread the fluid by centrifugal force. Rotation is continued while the fluid spins off the edges of the substrate, until a desired thickness of the film is achieved. The higher the angular speed of spinning, the thinner the film will be. The thickness of the film also depends on the concentration of the solution and the solvent used. Five drops of the PEDOT:PSS dispersion (Baytron® P VP AI 4083; H.C. Starck, from Hella Chemicals Pharmaceutical Import and Export Limited) solution were dropped onto the clean ITO glass substrates using a pipette. Vacuum hold down is engaged from the side mounted control of the spin coater. The PEDOT:PSS was deposited on the ITO coated glass substrate with two stages of spin, 500 rpm for 10 seconds and 1000 rpm for 30 seconds respectively. The thin films prepared were put on a 130 °C hot plate for 10 minutes to remove water from the blends.

3.1.3 P3HT:SQ3: PCBM deposition

These materials were used as received without further purification. The required amount of powder was weighed using a micro-scale in small vials. The powders were mixed and dissolved in chloroform solvents using disposable pipettes. The desired concentrations of the polymer,

fullerene and dye solutions were between 10 mg/ml and 20 mg/ml. P3HT:SQ3:PCBM was deposited on top of PEDOT:PSS film using the spin coating technique. The thin film was spin coated at 500 rpm for 10 seconds and 1000 rpm for 30 seconds.

3.1.4 Aluminium electrode deposition

The Varian High-Vacuum Electron Beam Evaporator-3117 (Materials Research Department, iThemba LABS, South Africa) was used to deposit the aluminium electrode. The Varian High-Vacuum Electron Beam Evaporator was pre-set to deposit 80 nm thicknesses using a high purity (99.99%) Al target placed into an intermetallic crucible liner. The instrument automatically sets the deposition rate, current and pressure as shown in Table 1.

Table 1: Evaporation beam deposition of 80 nm thick Aluminium.

Deposition rate (nm/s)	Current (mA)	Pressure (mBar)	Al thickness (nm)
0.30	120	2×10^{-6}	80
0.48	100	1×10^{-6}	80
0.60	130	2×10^{-6}	80
0.48	130	2×10^{-6}	80

3.2 CHARACTERIZATION OF THIN FILMS

3.2.1 Absorbance characteristics

Absorbance measurements of the prepared thin films were carried out using the Perkin Elmer Lambda 19 UV-Vis-NIR spectrometer (UNZA, Department of Physics). This spectrometer is used for optical absorbance and reflectance measurements in the wavelength range from 175 nm to 3300 nm. The project focused on the absorbance measurements because the first phase of photovoltaic conversion is the absorbance of light.

Regioregular P3HT, PCBM and Squarylium dye III (SQ3) were used as purchased from Hallo Chemicals Pharmaceutical Import and Export Limited without further purification. To study the effect of different amounts of SQ3 dye on the absorbance of P3HT:PCBM, 2 mg P3HT was blended with 2 mg PCBM and the mixture dissolved in 4 ml of chloroform. Then different amounts of SQ3 were added to the blend as shown in Table 2. The mixture was left overnight under magnetic stirring to maximize the mixing of the solution.

Table 2: P3HT:SQ3:PCBM blend ratios dissolved in 4.0 mL of chloroform.

SAMPLE	P3HT (mg)	PCBM (mg)	SQ3 (mg)
A	2.0	2.0	0.0
B	2.0	2.0	1.0
C	2.0	2.0	1.5
D	2.0	2.0	2.0

3.2.2 Surface morphological studies

Different thin films of P3HT:PCBM and P3HT:SQ3:PCBM were prepared. Veeco Nanoman AFM (Materials Research Department, iThemba LABS) was used to study the surface morphology of annealed and non-annealed prepared thin films. The major hardware components of the equipment are the scanner, with a closed (x-y) feedback loop which provides optimum positioning accuracy and the nano-scope controller which optionally incorporates a scanning tunnelling microscope. The Veeco Nanoman AFM also has an acoustic vibration isolation hood which not only shields the samples from atmospheric contaminants during imaging but is also an essential requirement for control of the ambient humidity during the local anodic oxidation process. The most important portion of the software components of the equipment is the lithography Nanoman software which guides the tip movement during the lithographic steps.

3.2.3 Thin film thickness measurements

The thin film thickness was measured using a Tencor Alpha-step Profilometer and Veeco Nanoman Atomic Force Microscope (AFM). 20 mg/mL P3HT: PCBM thin films in chloroform were prepared at different spin speeds as shown in Table 3. The film is scratched with a needle head to remove the active layer and to form a step. Then a surface profilometer or an AFM was used to measure the step height.

Table 3: 20 mg/mL P3HT: PCBM thin films in chloroform as a solvent.

P3HT:PCBM Sample	**Spin Speed (rpm)**
A	1200
B	1400
C	1600
D	2000

3.2.4 Thermal annealing studies

To study the effect of thermal annealing, thin films of P3HT:PCBM and P3HT:SQ3:PCBM were prepared on cleaned glass substrates. A hotplate was used to anneal thin films at 100 °C, 120 °C and 140 °C. Annealing time was 10 minutes for each selected temperature.

3.2.5 Electrical characteristics

The current density-voltage (*J-V*) characteristics were measured with the Keithley 2420 measurement unit and solar simulator shown in figure 9. The unit comprised of Keithley model 2420 source meter, a Keithley KPCI-488 IEEE-488 interface, a source illumination (AM 1.5 G), a temperature-controlled hold down chuck/test fixture, Keithley 7007-x IEEE-488 interface cable and test leads (4-wire) as well as 2-point adjustable contact probes. The simulator provides AM 1.5 solar irradiance with an intensity of 1 sun (100 mW/cm^2). The solar simulator

is to provide a controllable indoor test facility under laboratory conditions, used for the testing of solar cells.

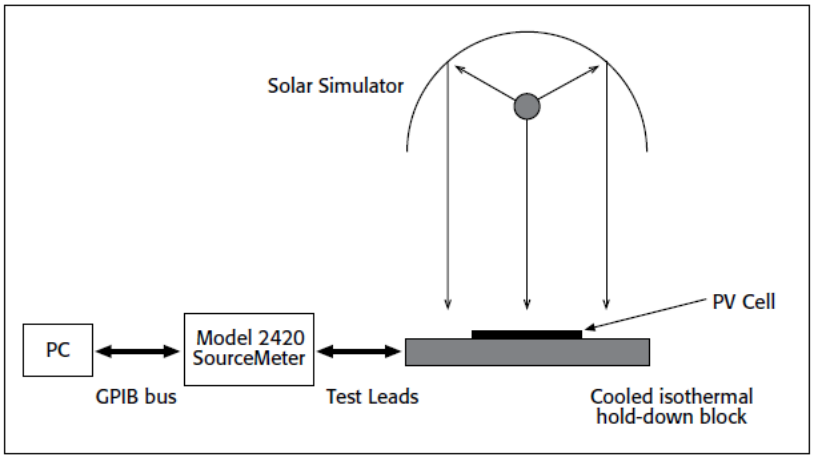

Figure 9: Keithley 2420 measurement unit.

The solar simulator provided 1 sun illumination (100 mW/cm^2) for the cell while a cooled, vacuum hold-down chuck, secures the cell and provides isothermal test conditions. The devices were illuminated through the ITO side. The working cell area was 0.8 cm^2 defined by the aluminium back electrode. The data collected at the end of the measurement was stored into text files for further analysis.

CHAPTER 4

RESULTS AND DISCUSSION

This chapter presents the results and discussion of the experiments which have been carried out in the laboratory during this project.

4.1 ABSORPTION CHARACTERIZATION OF ACTIVE MATERIALS

The spectral range of the optical absorption compared to the solar spectrum and absorption wavelength are the factors that affect the total number of absorbed photons by a solar cell active layer. The number of absorbed photons and the generated photocurrent in a solar cell increase when the absorption range and absorption peak value increase for the solar cell active layer. The absorption spectra of the active layer materials (P3HT, PCBM and SQ3 dye) compared to the standard solar illumination (AM 1.5 radiation) are shown in Figure10.

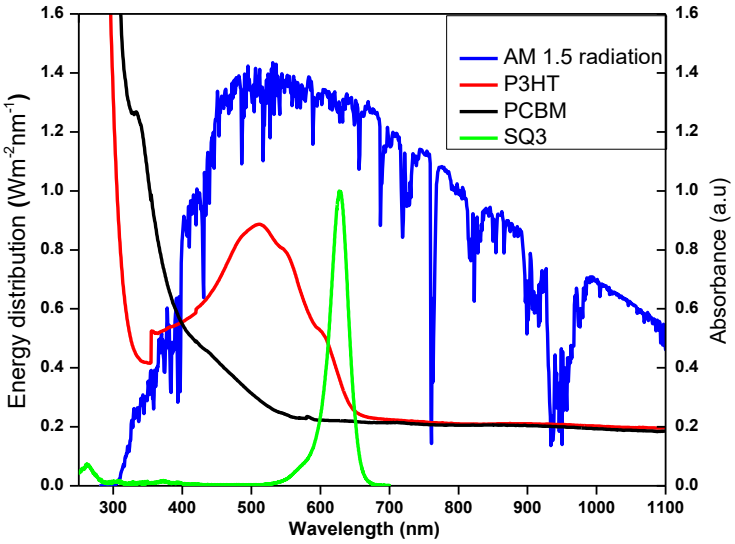

Figure 10: Absorption spectra for spin coated P3HT, PCBM and SQ3 dye thin films compared with the standard AM 1.5 solar spectrum.

Pure P3HT film showed peak absorbance at 511 nm with shoulders at 547 nm and 607 nm.

These three bands can be attributed to the pi to pi* (π-π*) transition of region-regular P3HT [97]. The pi to pi* transition is the promotion of electrons from a pi bonding molecular orbital (π) to a pi anti-bonding molecular orbital (π*). SQ3 showed peak absorbance at 627 nm. The number of photons absorbed in a solar cell active layer increases when the active layer absorbs in the red or near infra-red region of the solar spectrum, where there is the largest number of visible light photons. This is important because PSC converts visible light photons to electricity.

4.2 EFFECT OF SQ3 ON ABSORPTION

The contribution of SQ3 dye in light harvesting of P3HT:PCBM solar cell active layer was also evaluated by varying the concentration of SQ3 dye as reported in Table 4.

Table 4: Effect of SQ3 concentration on absorbance of P3HT:PCBM.

SQ3 mass (mg)	**PCBM mass (mg)**	**P3HT mass (mg)**	**SQ3 weight (%)**
2	20	20	4.76
4	20	20	9.09
6	20	20	13.04
8	20	20	16.67

Increasing the SQ3 content in the P3HT:PCBM blend increases light harvesting through the increase in absorbance and broadening of the absorption range as shown in Figure 11. Thus, the total number of photons absorbed by the solar cell active layer increases when SQ3 dye is added to the P3HT:PCBM blend. SQ3 raised the light harvesting of the P3HT:PCBM blend by appearing as a donor material and increased the site for exciton dissociation in the blend. This is because the HOMO of SQ3 is located in-between the HOMOs of P3HT and PCBM, with a similar situation for the LUMO) levels.

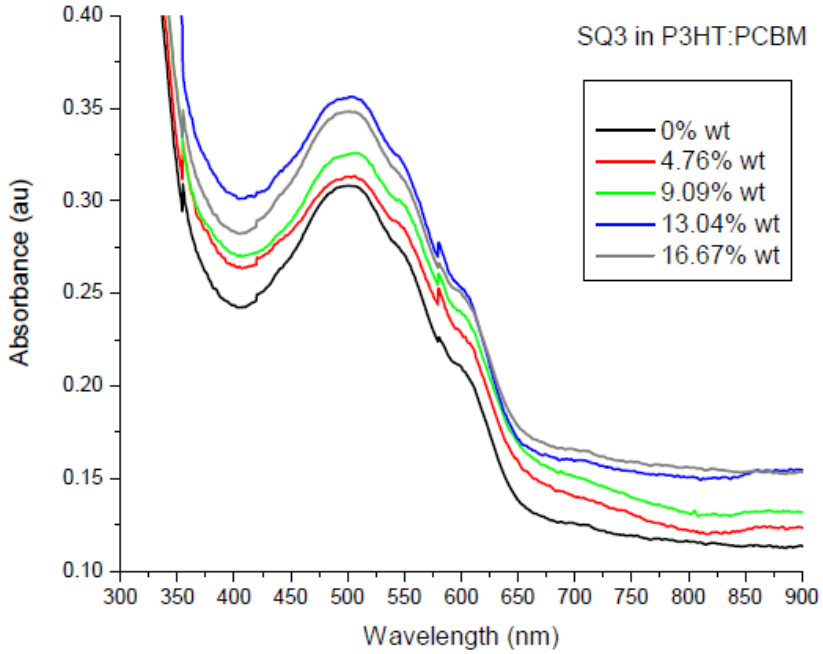

Figure 11: Absorbance spectra of pristine P3HT:PCBM (black) and P3HT:SQ3:PCBM blend films.

Consequently the initial excitation leads to two possible routes for current generation: (i) photo induced charge transfer between P3HT and PCBM, (ii) Förster resonance energy transfer (FRET) excitation of P3HT to SQ3 followed by charge dissociation. FRET is a non-radiative energy transfer process that acts through long range dipole-dipole interaction between donor and acceptor molecules. The strength of this interaction is dependent on the overlap of the donor emission (P3HT) and the acceptor absorption (SQ3). However, there is a decrease in absorbance when the concentration of SQ3 was 16.67 %. The decrease may be attributed to the disturbed interpenetrating network between P3HT and PCBM with the relative decrease in the P3HT:PCBM content with the high concentration of SQ3, which hinders charge transportation.

4.3 EFFECT OF THERMAL ANNEALING

The UV-Vis absorption spectrometer was used to study the effect of thermal annealing on spin coated P3HT:PCBM thin films and the results are shown in Figure 13. The untreated thin

film showed a peak absorbance of 0.30 and peak absorption wavelength is at 501 nm with shoulders at 545 nm and at 597 nm.

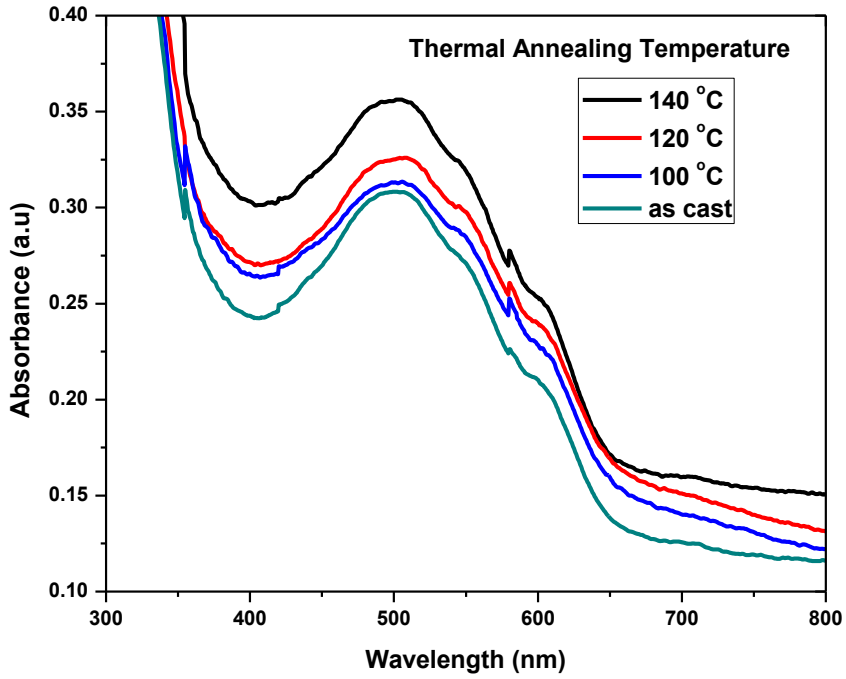

Figure 12: Effect of thermal annealing on spin coated P3HT:PCBM thin films.

Table 5: Effect of increasing thermal annealing temperature on peak absorbance.

Thermal annealing temperature (ºC)	**Peak absorbance (a.u)**
100	0.31
120	0.32
140	0.36

Table 5 is derived from Figure 12 and shows how the peak absorbance increased with an increase in thermal annealing. It is deduced that the annealing at 100 ºC increased peak absorbance from 0.30 to 0.31 arbitrary units (a.u) while annealing at 140ºC increased peak absorbance to 0.36 a.u. Thin films treated at 140°C show a red shift of peak absorption wavelength from 501 nm to 510 nm and the shoulders shift to 604 nm. Annealing at a

temperature greater than the glass transition temperature (T_g) of P3HT allowed the polymer chains to reorganize and the fullerene molecules to freely diffuse into the composite and reorder in a more thermodynamically favourable way. The glass transition temperature of P3HT has been reported to be between 110 °C to 125 °C [98]. The annealing time for all the above temperatures was 10 minutes. The red shift is ascribed to increased inter-chain interaction among the P3HT chains arising from annealing. Therefore, annealing lowered the band-gap and increased the optical π-π* transition, which is an indication of the formation of crystallites [99].

4.4 MORPHOLOGY STUDIES

In order to investigate the surface morphologies of the fabricated films, the variation in the surface roughness of the film was monitored by means of the atomic force microscope (AFM). ITO coated glass was used as received while PEDOT:PSS was spin-coated on cleaned glass at 1000 rpm and a concentration of 20 mg/ml P3HT:PCBM was spin coated from a chloroform solution at 1400 rpm. Root mean square roughness (R_{rms}) was obtained from the Nanoscope AFM imaging software. R_{rms} is a representation of surface roughness. R_{rms} is the root mean square average of the profile height deviations from the mean line, recorded within the evaluation length. The R_{rms} is given by equation (10).

$$R_{rms} = \sqrt{\frac{1}{L}\int_0^L Z(x)^2\,dx} \tag{10}$$

Here, L is the evaluation length and $Z(x)$ is the profile height function.

AFM was used to study the surface morphology of ITO, PEDOT:PSS and P3HT:PCBM on glass substrates. The results are as shown in Figure 13.

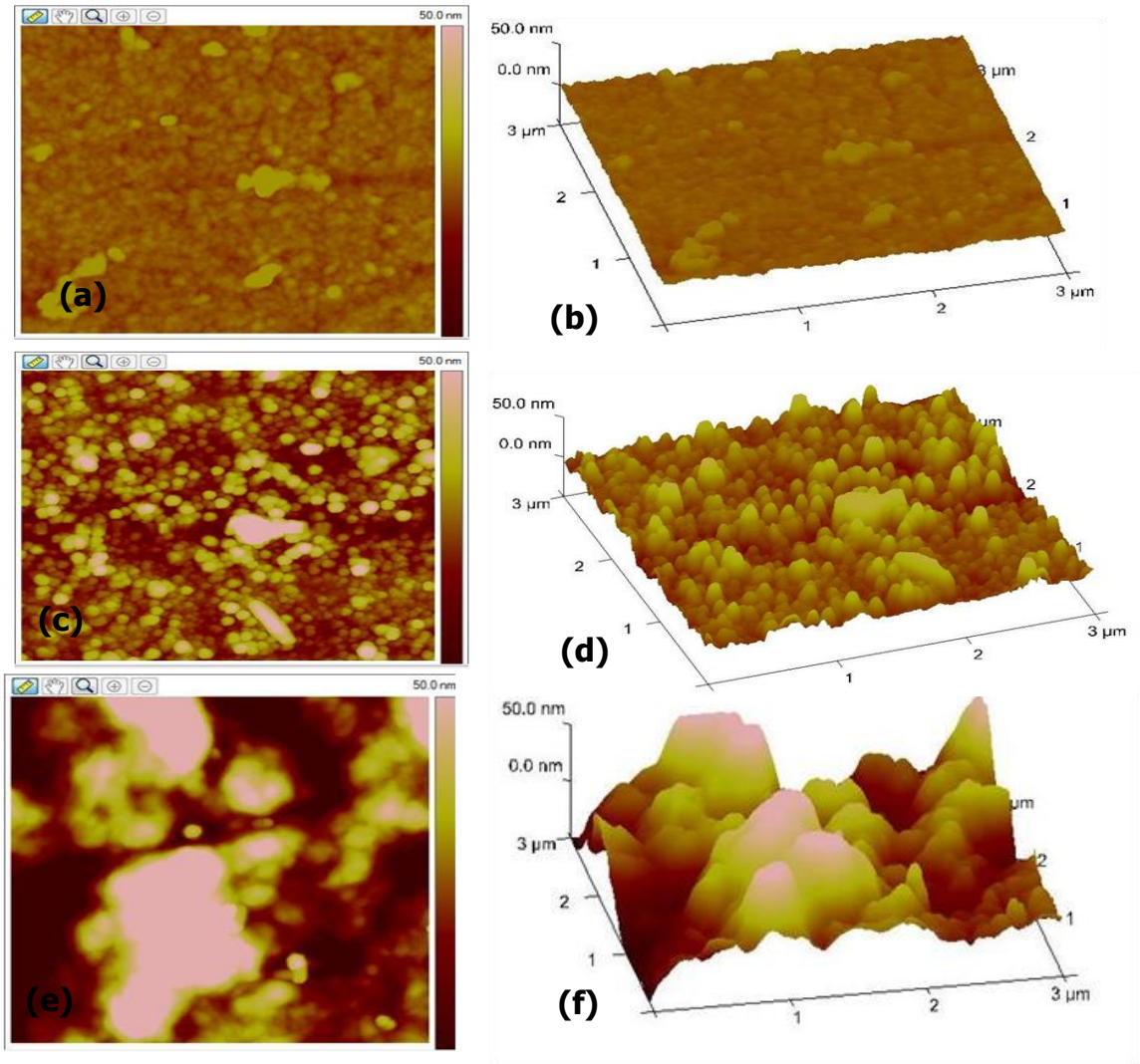

Figure 13: AFM images (3 µm x 3 µm) of ITO coated glass (a, b), PEDOT: PSS (c, d) and P3HT:PCBM (e,f).

The corresponding values of R_{rms} of the AFM images of figure 13 are derived from the AFM imaging software and are tabulated in table 6. From Table 6, P3HT:PCBM had a rougher surface compared to PEDOT:PSS and ITO respectively.

Table 6: Root mean square roughness of AFM images of Figure 13.

	(a) and (b)	**(c) and (d)**	**(e) and (f)**
$\boldsymbol{R_{rms}}$ (nm)	1.94	8.03	22.7

To study the effect of SQ3 on the morphology of P3HT:PCBM active layer, AFM images were taken on P3HT:PCBM blend films with and without SQ3 as shown in Figure 14. The AFM height images of Figure 14 show the P3HT:PCBM blend films with and without SQ3.

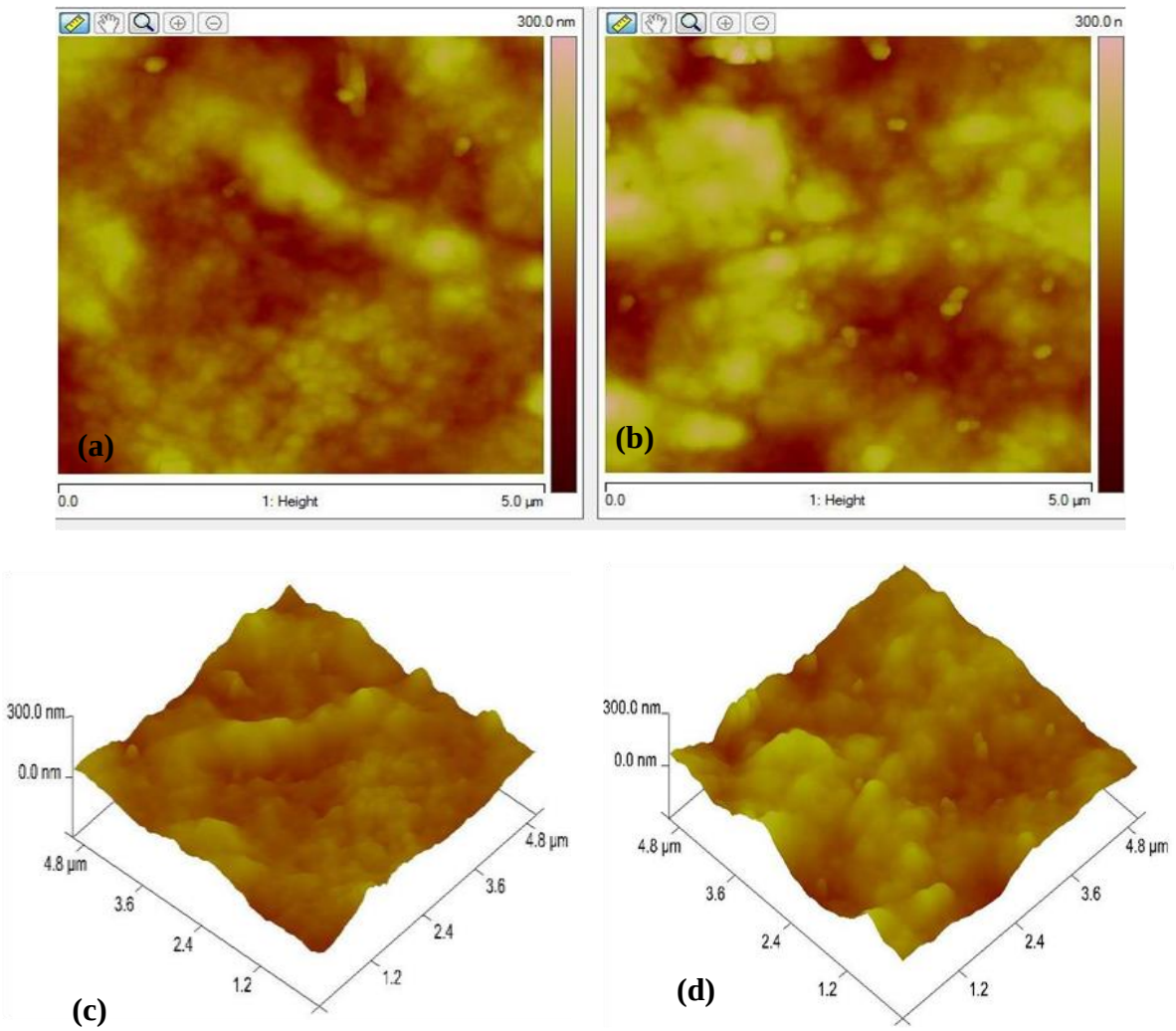

Figure 14: 2 Dimension AFM images (5µm x 5µm) of P3HT:PCBM (a) and PCBM:SQ3:PCBM (b), 3 Dimension AFM images (5µm x 5µm) of P3HT:PCBM (c) and PCBM:SQ3:PCBM (d).

Pristine P3HT:PCBM blend film show a smooth surface while P3HT:SQ3:PCBM blend film shows a much rougher one. The root-mean-square roughness (R_{rms}) values of the

P3HT:PCBM and P3HT:SQ3:PCBM films are 1.54 nm and 2.41 nm at the 5 μm × 5 μm scan size, respectively as shown on the Nanoscope AMF scan images.

Figure 15 shows the AFM images used to study the combined effect of thermal annealing and the SQ3 to the morphology of the P3HT: PCBM active layer.

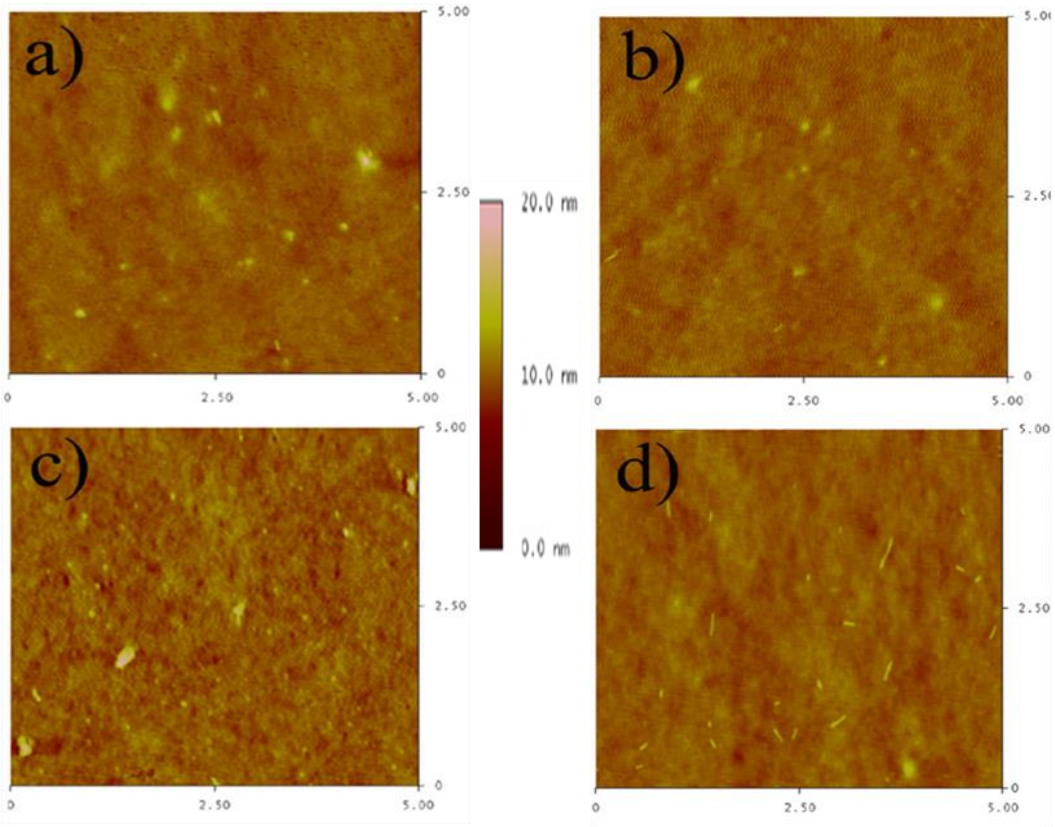

Figure 15: AFM (5 nm x 5 nm) images of P3HT: PCBM blend films of (a) without SQ3 additive, (b) without SQ3 additive and with thermal annealing (c) with the additive of SQ3 (d) with the additive of SQ3 and with thermal annealing.

The effect of SQ3 and annealing on the R_{rms} values of P3HT:PCBM is reported in table 7.

Table 7: Effect of SQ3 and annealing on R_{rms} values of P3HT:PCBM.

AFM image	COMPOSITION	ANNEALED (140 °C)	R_{rms} (nm)
(a)	P3HT: PCBM	NO	0.38
(b)	P3HT:PCBM	YES	0.75
(c)	P3HT:SQ3: PCBM	NO	0.91
(d)	P3HT:SQ3: PCBM	YES	0.80

Table 7 is a summary of R_{rms} values of the AFM images of Figure 15. In Figure 15, image (a) is the control and has R_{rms} = 0.38 nm. Annealing image (a) at 140 °C for 10 minutes increased R_{rms} to 0.75 nm as shown by image (b). This increase in roughness is associated with the increased order in the P3HT phase after annealing at 140 °C. The addition of SQ3 to P3HT:PCBM increased R_{rms} from 0.38 nm to 0.91 nm as image (c) shows. Image (c) also shows a much coarser texture with broad hill-like features compared to the other films. However, the addition of SQ3 to P3HT:PCBM and annealing at 140 °C for 10 minutes reduced R_{rms} to 0.80 nm as shown in (d). This slight reduction suggests reduced crystallinity and suggests that SQ3 molecules prefer to reside at the interface between P3HT and PCBM.

4.5 FILM THICKNESS CHARACTERIZATION

Thin film thickness measurements are important because the absorption coefficient of a layer is related to its thickness. Figure 16 shows the dependence of spectral absorbance on wavelength as deposition speed is varied during spin-coating.

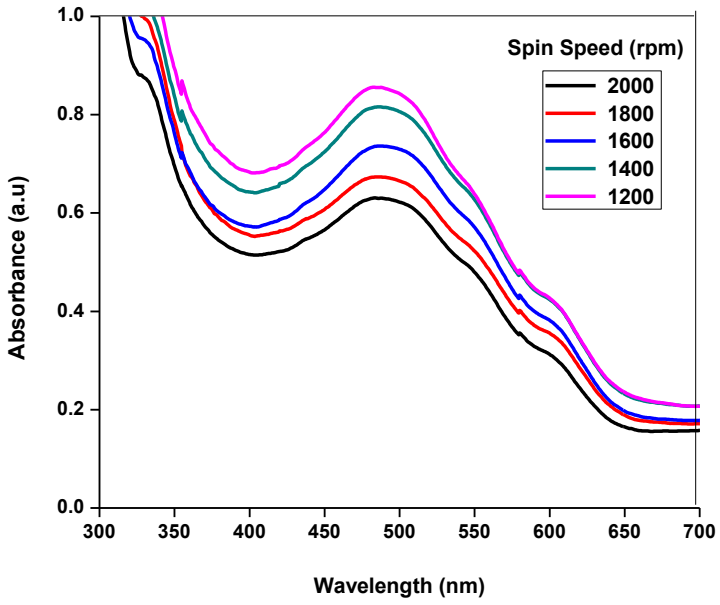

Figure 16: Absorbance spectra of P3HT:PCBM blend films spin coated at different speeds.

Table 8 is extracted from Figure 16 and shows the effect of spin-speed on thin film thickness.

Table 8: Spin-speed versus peak absorbance

Spin-speed (rpm)	**Peak absorbance (a.u)**
1200	0.85
1400	0.80
1600	0.73
1800	0.67
2000	0.63

Clearly, increasing the spin-coating speed resulted in a reduction in the absorbance. The same films of Figure 16 were scratched with a needle head to form a step. Then a Tencor Alpha-step profilometer was used to determine the thickness and the results are shown in Table 9.

Table 9: The effect of spin-speed on thin film thickness.

Spin coating speed (rpm)	1200	1400	1600	1800	2000
Thickness (nm)	280	220	190	150	120

The data of Table 9 was used to plot Figure 17.

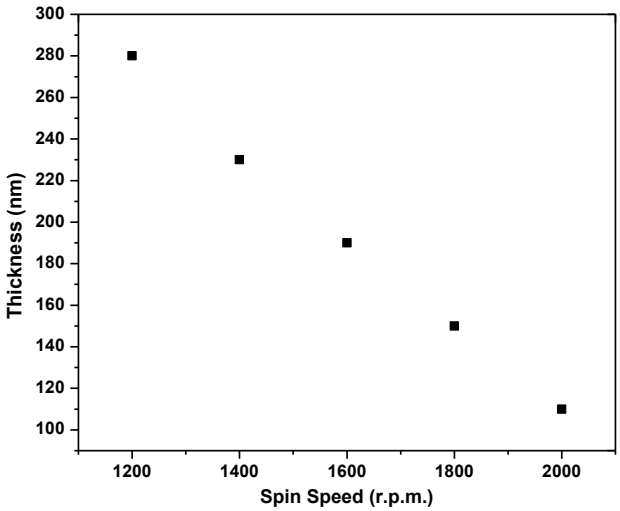

Figure 17: Spin coating speed verses thin film thickness for spin coated 20mg/mL P3HT:PCBM blend film.

Figure 17 shows that film thickness is inversely proportional to the spin-coating speed. The need to mix two or more materials in a BHJ further limits charge transport and therefore layer thickness. Thicker active layers absorb more light and generate more excitons but have low collection efficiency compared to thinner layers. However, the excitons must be separated and free charge carrier pairs must be collected at the electrodes in order to generate a photocurrent. Thick active layers allow charges to recombine before reaching the electrodes, leading to lower photocurrent. They can also increase domain size, which lowers exciton dissociation rates. Thicker layers have less favourable morphological organization, especially next to the hole-collecting electrode, and as a result produce poorly functioning devices.

4.6 ALUMINIUM ELECTRODE CHARACTERIZATION

The aluminium (Al) layer (cathode) was deposited by evaporation beam and defines the active area of the polymer solar cell. Different thicknesses of aluminium were deposited and characterised for absorbance and resistance per square centimetre. A digital multi-meter was used to measure the resistance and the results are summarised in Table 10.

Table 10: Thickness versus resistance for evaporation beam deposited Aluminium.

Thickness (nm)	**Resistance (ohm*cm^{-1})**
20	20.0
50	10.3
80	6.0
100	4.7
120	3.5

The data of Table 10 is plotted in Figure 18.

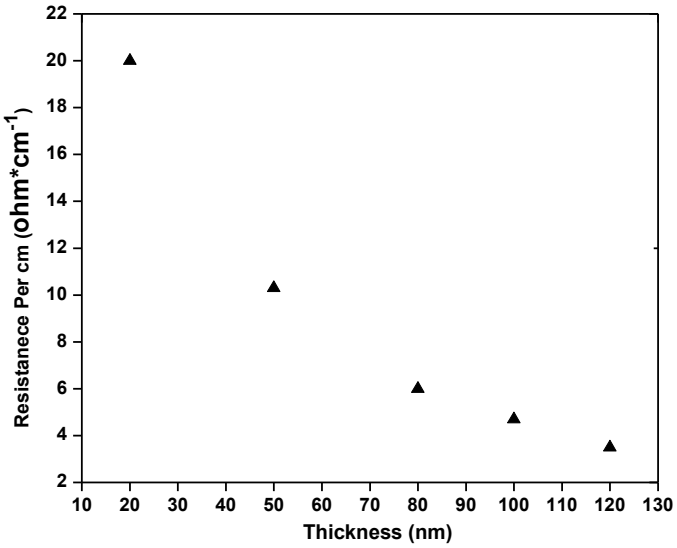

Figure 18: Thickness verses resistance per cm for the e-beam deposited Al.

The aim of this characterization was to determine the minimum thickness required for Al to be used as a cathode. The good Al cathode must be smooth, dimple free and with a low resistance. It is observed from Figure 18 that resistance per centimetre of Al reduced as the thickness increased. Therefore, a thickness between 80 nm and 120 nm is ideal for Al cathode for PSC application.

4.7 ELECTRICAL CHARACTERISATION

Solar cell electrical characteristics are determined by measuring the current density-voltage (*J-V*) characteristics, both in the dark and under illumination. The *J-V* characteristics in the dark correspond to the measurement of the current produced due to the application of a varying voltage in both the forward and reverse directions. The *J-V* characteristics under illumination are carried out for the purpose of studying the electrical properties of the PSC device. The method used to measure current density-voltage characteristics for the solar cells applied a fixed illumination (100 mW/cm^2) and a resistive load which was varied between the short circuit and open circuit conditions. Then the voltage across the solar cells terminals and

the current out of these terminals was measured using the Keithley source measurement unit. This method of measurement applies to solar cells in its normal photovoltaic mode of operation. Origin software was used to plot the *J-V* curves shown in Figure 19. The fabricated polymer solar cell device structure is shown Table 11 and their corresponding *J-V* curve is shown in Figure 19. Thermal annealing was done at a temperature of 140˚C.

Table 11: Polymer solar cell device configurations.

Solar Cell	Device Configuration	Illumination	Annealing
A	ITO/PEDOT:PSS/P3HT:SQ3:PCBM/Al	NO	NO
B	ITO/PEDOT:PSS/P3HT:PCBM/Al	YES	NO
C	ITO/PEDOT:PSS/P3HT:SQ3:PCBM/Al	YES	NO
D	ITO/PEDOT:PSS/P3HT:PCBM/Al	YES	YES
E	ITO/PEDOT:PSS/P3HT:SQ3:PCBM/Al	YES	YES

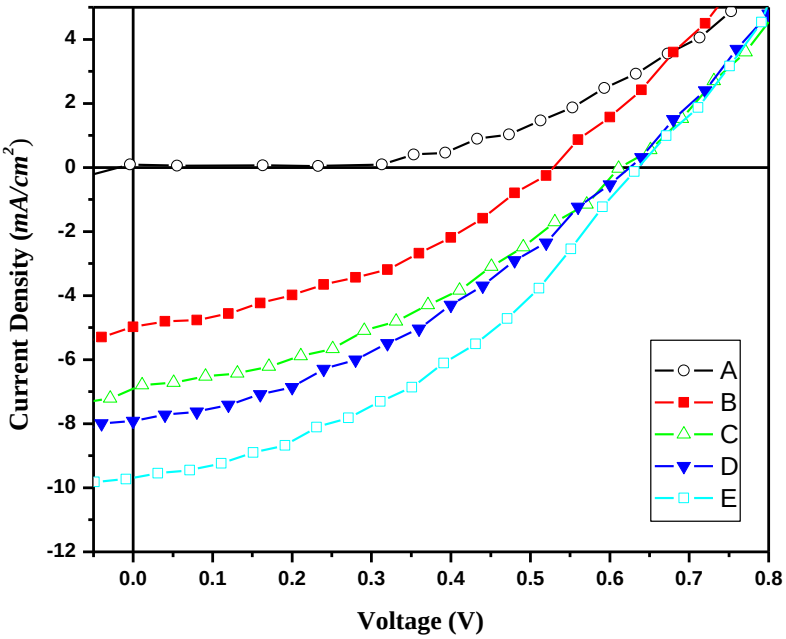

Figure 19: Current density-voltage (*J-V*) curves obtained for solar cells under AM 1.5 solar spectrum simulation (light) at irradiation intensity of 100 mW/cm^2.

The open circuit voltage (V_{oc}), short circuit current (J_{sc}), maximum current (J_{max}) and maximum voltage (V_{max}) were derived from Figure 19. The maximum power point (P_{max}), fill factor and power conversion efficiency (η) were calculated using equations (6), (7) and (9) respectively. The electrical parameters of PSCs determined from Figure 19 are summarised in Table 12.

Table 12: The electrical parameters of the fabricated PSCs.

Solar Cell	V_{oc} **(V)**	J_{sc} **(mA)**	V_{max} **(V)**	J_{max} **(mA)**	P_{max}	***FF***	η **(%)**
B	0.53	5.78	0.32	3.39	1.08	0.35	1.3
C	0.61	6.88	0.37	4.29	1.59	0.38	2.5
D	0.62	7.88	0.36	5.04	1.81	0.37	2.8
E	0.64	9.68	0.36	6.86	2.41	0.40	3.9

From Tables 11 and 12, the addition of SQ3 to P3HT:PCBM increased the V_{oc} from 0.61 V to 0.62 V while the J_{sc} increased from 5.78 mA to 6.88 mA. The addition of SQ3 and annealing increased open circuit voltage from 0.61 V to 0.64 V while the J_{sc} increased from 5.78 mA to 9.68 mA. The increase in J_{sc} and V_{oc} can be attributed to the high absorbance of SQ3 in the near-infrared region which broadens the spectral absorption of the solar cells. Annealing promotes phase mixing between P3HT, PCBM and SQ3 and this also contributed to the increase in J_{sc} and V_{oc}. The control device fabricated from the P3HT:PCBM blend active layer has V_{oc} = 0.53 V, J_{sc} = 5.78 mA and FF = 35% and η = 1.3 %, as shown in figure 13. The addition of SQ3 improved η to 2.5 % while annealing improved it to 2.8 %. The combined effect of thermal annealing and addition of SQ3 improves η to 3.9 %.

This is the first time SQ3 is incorporated in a P3HT:PCBM active layer material for PSC application. The main challenge in the construction of the PSC was the lack of the glove box. Spin coating of the active layer should have been done in a glove box with a controlled nitrogen atmosphere to prevent degradation due to moisture, humidity and oxygen. Furthermore, the metallic electrode of the PV device consisted only of aluminium instead of the optimum bilayer of either gold or silver (due to their intrinsic stability in air) and aluminium.

The study illustrates that spin coating is a powerful technique for the fast, inexpensive fabrication of polymer solar cell devices while retaining nano-scale control of the film thickness. The application of this technique to the fabrication of organic solar cells further increases the strong potential that these devices have for practical use.

CHAPTER 5

CONCLUSION AND RECOMMENDATIONS

This chapter presents the conclusions of the research described in the dissertation and recommendations for future work.

5.1 CONCLUSION

Organic solar cells based on P3HT:PCBM as the active layer were prepared. The effect of thermal annealing and dye loading using Squarylium III dye was evaluated. Thermal annealing led to thermodynamically driven reorganization of the morphology of the P3HT:SQ3:PCBM active layer. Annealing increases inter-chain interactions resulting in greater delocalization of electrons leading to lowering in the band gap. Lowering of the band gap enables more π–π* transitions hence the red shift observed. The light harvesting capacity of the active layer is enhanced due to better overlap with the solar spectrum so that more photons are harvested and more excitons are created. Therefore, by thermal annealing, the P3HT and SQ3 absorb a larger number of photons and consequently increase the generation of charge carriers in the solar cells. Furthermore, thermal annealing optimizes the interfacial contact between the metal electrode and the active layer thereby reducing recombination losses. Additionally, thermal annealing increases the number of charges collected at the electrode. The contribution of the SQ3 dye in the photocurrent is attributed to its pronounced contribution in the light harvesting of the solar cell active layer, which increases on raising the dye loading in the active layer blends. The optimum dye loading was found to be at 13.04 % with a significant increase in the maximum peak absorbance, from 0.31 to 0.36 a.u. The absorption range was also observed to broaden (400 – 700 nm) extending to the near infra-red. The red shift observed on incorporating SQ3 dye is ascribed to increased P3HT stacking resulting in lowering of the band gap and hence increasing π-π* transitions. The SQ3 dye molecules also provide a second exciton generation system and charge transfer me π-π* mechanism. The combined effects of thermal

annealing and inclusion of dye resulted in an increase in the V_{oc}, J_{sc}, FF and η values compared to the control device. V_{oc}, J_{sc}, FF and η in the control P3HT:PCBM were 0.53 V, 5.78 mA 0.35 and 1.3 % which changed to 0.64 V, 9.68 mA, 0.40 and 3.9 % respectively in P3HT:SQ3:PCBM blends. This represents a threefold increase in the photo-conversion efficiency η.

5.2 RECOMMENDATIONS FOR FUTURE WORK

The potential to increase the photo-conversion efficiency has clearly been demonstrated in this work through thermal annealing and inclusion of small dye molecules which improved the light harvesting capacity of the active layer. One of the challenges of PSCs is that the thickness of the active layer is limited to about 200 nm to avoid recombination of charges. This therefore also limits the amount of light that is absorbed. There is a threshold for the amount of dye that can be added without compromising the optimum morphology of the active layer. It is therefore desirable to investigate alternative means of increasing the light harvesting capacity. Future work could therefore consider the use of metal nanoparticles to achieve enhanced absorption through plasmonic effects and also improving transparency of the PEDOT:PSS layers which takes in about 20 % of the incident light.

REFERENCES

[1] BP. (2008) “Statistical review of world energy.” Available: http://www.bp.com/productlanding.do?category ID=6929&contentID=7044622

[2] Worldwatch Institute, “State of the world – into a warming world,” (2009) Available: http://www.worldwatch.org/files/pdf/SOW09_chap3.pdf/

[3] U.S. Energy Information Administration, (2008). “International energy outlook,” Available: http://www.eia.doe.gov/oisf/ieo/index.html”.

[4] W. Bartok and A. F. Sarofim, (1991) Fossil Fuel Combustion: A Source Book. New York: John Wiley & Sons, Inc.

[5] J. Halme (2002) “Dye-sensitized Nanostructured and Organic Photovoltaic Cells,” Technical Review and Preliminary Tests, Master of Science Thesis, Helsinki University of Technology: 8-9.

[6] United Nations (2009) Department of Economic and Social Affairs, World Population. Prospectus Revision, June 2013, http://esa.un.org/unpd/wpp/index.html

[7] E. McLamb, (2011) “Fossils fuels vs. renewable energy resources”: Available: http://www.ecology.com/2011/09/06/fossil-fuels-vs-renewable-energy-resources/.

[8] M. Meinshausen, N. Meinshausen, W. Hare, S. C. B. Raper, K. Frieler, R. Knutti, D. J. Frame and R. Allen (2009) “Greenhouse-gas emission targets for limiting global warming to 2 ^{o}C,” *Nature* 458 (7242): 1417-1456.

[9] Environmental and Ethical Aspects of Long-lived Radioactive Waste Disposal. “Proceedings of an International Workshop organised by the Nuclear Energy Agency in cooperation with the Environment Directorate”, Paris, 1 -2 September 1994, OECD Documents.

[10] C. M. Haanyika (2008) “Rural electrification in Zambia: A policy and institutional analysis,” Energy Policy, 36(3), 1044-1058.doi:DOI:10.1016/j.enpol.2007.10.31

[11] Y. J. Cheng, S. H. Yang and C. S. Hsu, (2009). "Synthesis of conjugated polymers for organic solar cell applications," *Chemical Reviews,* 109 (11): 5868-5923.

[12] V. D. Mihailetchi, L. J. A. Koster, P. W. M. Blom, C. Melzer, B. De Boer, J. K. J. Van Duren and R. A. J. Janssen (2005) "Compositional dependence of the performance of poly(p-phenylenevinylene): methanofullerene bulk-hetero-junction solar cells," *Advanced Function Materials,* 15: 795–801.

[13] F.C. Krebs (2009) "Fabrication and processing of polymer solar cells: a review of printing and coating techniques," Solar Energy Materials for Solar Cells 93: 394–412.

[14] C. J. Brabec and J. R. Durrant (2008) "Solution-processed organic solar cells," MRS Bulletin, 33: 670-675.

[15] J. Y. Kim, K. Lee, N. E. Coates, D. Moses, T. Q. Nguyen, M. Dante and A. J. Heeger (2007) "Efficient tandem polymer solar cells fabricated by all-solution processing," *Science,* 317:222–225.

[16] B. Zimmermann, M. Glatthaar, M. Niggemann, M. K. Riede, A. Hinsch, A. Gombert, (2007) "ITO-free wrap through organic solar cells a module concept for cost-efficient reel-toreel production," *Solar Energy Materials and Solar Cells*, 91: 374–378.

[17] S. E. Shaheen, C. J. Brabec, and N. S. Sariciftci (2001) "2.5% efficient organic plastic solar cells," *Applied Physics Letters,* 78:841.

[18] F. Padinger, R. S. Rittberger, and N. S. Sariciftci (2003) "Effects of postproduction treatment on plastic solar cells," *Advanced Function Materials*, 13:85.

[19] J. Peet, J. Y. Kim, N. E. Coates, W. L. Ma, D. Moses, A. J. Heeger, and G. C. Bazan, (2007) "Efficiency enhancement in low-bandgap polymer solar cells by processing with alkane dithiols," Natural Materials, 6:497.

[20] C. Gueymard (2004) "The sun's total and spectral irradiance for solar energy applications and solar radiation models," *Solar Energy*, 76(4): 423-453.

[21] S. H. Park, A. Roy, S. Beaupre, S. Cho, N. Coates, J. S. Moon, D. Moses, M. Leclerc, K. Lee, and A. J. Heeger (2009) "Bulk hetero-junction solar cells with internal Quantum efficiency approaching 100%." *Natural Photonics,* 3:297.

[22] B. A. Gregg and M. C. Hanna (2003) "Comparing organic to inorganic photovoltaic cells: Theory, experiment and simulation," *Journal of Applied Physics*: 3605-3614.

[23] V. Shrotriya, G. Li, Y. Yao, T. Moriarty, K. Emery, and Y. Yang (2006) "Accurate measurement and characterisation of organic solar cells." *Advanced Function Materials,* 16: 2016.

[24] W. Shockley and H. J. Queisser (1961) "Detailed balance limit of efficiency of p-n junction solar cells." *Journal of Applied Physics,* 32: 510.

[25] P. Schilinsky, C. Waldauf, J. Hauch, and C. J. Brabec (2004) "Simulation of light intensity dependent current characteristics of polymer solar cells." *Journal of Applied Physics,* 95:2816.

[26] M. A. Green (1986) "Solar Cells: Operating Principles, Technology and System Applications," University of New South Wales, Sydney.

[27] H. Hoppe and N. S. Sariciftci, (2006) "Morphology of polymer/fullerene bulk heterojunction solar cells," *Journal of Material Chemistry*, 16: 45–61.

[28] C. Jincan (1996) "Thermodynamic analysis of a solar driven thermoelectric generator," *Journal of Applied Physics,* 79:5.

[29] H. Hoppe and N. S. Sariciftci (2006) "Morphology of polymer/fullerene bulk heterojunction solar cells," *Journal of Material Chemistry*, 16: 45–48.

[30] C. Lungenschmied, G. Dennler, H. Neugebauer, S.N. Sariciftci, M. Glatthaar, T. Meyer and A. Meyer (2007) "Flexible, long-lived, large-area, organic solar cells," *Solar Energy Materials and Solar Cells*, 91: 379–384.

[31] W. L. Ma, C. Y. Yang, X. Gong, K. Lee and A. J. Heeger (2005) “Thermally stable, efficient polymer solar cells with nanoscale control of the interpenetrating network morphology,” *Advanced Function Materials*, 15:1617–1622.

[32] W. Ma, C. Yang and A. J. Heeger (2007) “Spatial Fourier-transform analysis of the morphology of bulk heterojunction materials used in ‘plastic’ solar cells.” *Advanced Materials,* **19**(10), 1387-1390.

[33] L. S. Hung, C. W. Tang, and M. G. Mason (1996) “Enhanced electron injection in organic electroluminescence devices using an al/lif electrode,” *Applied Physics Letters*, 70: 2.

[34] L. A. A. Pettersson, L. S. Roman and O. Inganas (1999) “Modeling photocurrent action spectra of photovoltaic devices based on organic thin films,” *Journal of Applied Physics*, 86 (1), 487-496.

[35] T. Tsuzuki, Y. Shirota, J. Rostalski, D. Meissner (2000) *Solar Energy Materials and Solar Cells* 61 (15): 1.

[37] C. J. Brabec (2008) “Design rules for donors in bulk-hetero-junction tandem solar cells towards 15% energy-conversion efficiency,” *Advanced Materials*, 20: 579–583.

[38] M. C. Scharber, D. Wuhlbacher, M. Koppe, P. Denk, C. Waldauf, A.J. Heeger, and C. J. Brabec (2006). “Design rules for donors in bulk-hetero-junction solar cells—towards 10% energy-conversion efficiency,” *Advanced Materials*, 18: 789–794.

[39] L. S. Hung, C. W. Tang, and M. G. Mason (1996) “Enhanced electron injection in organic electroluminescence devices using an al/lif electrode,” *Applied Physics Letters*, 70 (2):152-154.

[40] P. Schilinsky, C. Waldauf, J. Hauch, and C. J. Brabec (2004) “Simulation of light intensity dependent current characteristics of polymer solar cells,” *Journal of Applied Physics*, 95:2816.

[41] M. A. Green (1986) Solar Cells: Operating Principles, Technology and System Applications, University of New South Wales, Sydney.

[42] H. Hoppe and N. S. Sariciftci (2006) "Morphology of polymer/fullerene bulk heterojunction solar cells," *Journal of Material Chemistry,* 16: 55–61.

[43] B. Kippelen and J. L. Bredas (2009) "Organic photovoltaics," *Energy Environmental Sciences,* 2: 251–261.

[44] T. Tsuzuki, Y. Shirota, J. Rostalski, D. Meissner (2000) "The effect of fullerene doping on photoelectric conversion using titanyl pthalocyanine and a perylene pigment," *Solar Energy Materials and Solar Cells* 61: 1.

[45] M. Girtan and M. Rusu (2010) "Role of ITO and PEDOT:PSS in stability/degredation of polymer:fullerene bulk hetero-junctions solar cells," *Solar Energy Materials and Solar Cells,* 94(3): 446-450.

[46] M. C. Scharber, D. Wuhlbacher, M. Koppe, P. Denk, C. Waldauf, A. J. Heeger, and C. J. Brabec (2006) "Design rules for donors in bulk-hetero-junction solar cells towards 10% energy-conversion efficiency," *Advanced Materials,* 18: 789–794.

[47] S. Sreejith, P. Carol, P. Chithra and A. Ajayaghosh (2008) "Squaraine dyes: a mine of molecular materials," *Journal of Materials Chemistry,*18(3):264–274.

[48] J. Griffiths and J. Mama (2000) "pH-dependent absorption and fluorescence of hydroxyaryl-squarylium dyes," *Dye Pigments,* 44: 9-17.

[49] J. Zhao, A. Swinnen, G. van Assche, J. Manca, D. Vanderzande, and B. van Mele (2009) "Phase diagram of P3HT/PCBM blends and its implication for the stability of morphology," *Journal of Physical Chemistry B,* 113(6):1587-1591.

[50] K. Y. Law (1987) "Squaraine chemistry. Effects of structural changes on the absorption and multiple fluorescence emission of bis[4-(dimethylamino) phenyl squaraine and its derivatives," *Journal of Physical Chemistry,* 91: 5184-5193

[51] M. Grätzel (2001) “Photoelectrochemical Cells,” Nature, November 1.

[52] C. W. Tang (1986). “Two layer-organic photovoltaic cell,” *Applied Physics Letters,* 4 8: 182-185.

[53] E. C. P. Smits, S. Setayesh, T. D. Anthopoulos, M. Buechel, W. Nijssen, R. Coehoorn, P. W. Blom, B. de Boer and D. M. de Leeuw (2007) “Near-infrared light emitting ambipolar organic field effect transistors,” *Advanced Materials,* 19: 734–738.

[54] T. Hribernik (2013) “Organic solar cell characterization systems based on photovoltage spectrocopy,” Master’s thesis, University of Maribor, Faculty of Electrical Engineering and Computer Science.

[55] US Department of Energy: Energy Efficiency and Renewable Energy. “The History of Solar cell.” http://www1.eere.energy.gov/solar/pdf/solar_timeline.pdf.

[56] M. J. Kerr, P. Campbell, and A. Cuevas (2002) “Lifetime and efficiency limits of Crystalline silicon solar cells,” in Proceedings of the 29th IEEE Photovoltaic Specialists Conference, 438 – 441.

[57] J. Zhao, A. Wang, and M. A. Green (1999) “24·5% Efficiency silicon PERT cells on MCZ substrates and 24·7% efficiency PERL cells on FZ substrates.” *Progress in Photovoltaics: Research and Applications,* 7 (6): 471 –474.

[58] W. Smith (1873) “The action of light on selenium,” *Journal of the Society of Telegraph Engineers,* 2: 32.

[59] C. W. Tang, S. A. Van Slyke, and C. H. Chen (1989) “Electroluminescence of doped organic thin-films,” *Journal of Applied Physics,* 69(15): 3610-3616.

[60] W. Shockley, (1949). “The Theory of p-n junctions in semiconductors and p-n junction transistors,” *Bell System Technical Journal,* 28(3): 435.

[61] D. M. Chapin, C. S. Fuller, G. L. Pearson (1954) “A new Silicon p-n Junction

Photocell for Converting Solar Radiation into Electrical Power," *Journal of Applied Physics,* 25(5): 676- 677.

[62] A. Einstein (1905) "About the Production and Transformation of a relevant history heuristschen spot light," *Annals of Physics,* 17: 132.

[63] G. Li, V. Shrotriya, J.S. Huang, Y. Yao, T. Moriarty, K. Emery, Y. Yang (2005) "High-efficiency solution processable polymer photovoltaic cells by self-organization of polymerblends," *Natural Materials,* 4: 864–868.

[64] J. Y. Kim, S. H. Kim, H. Lee, K. Lee, W. Ma, X. Gong, A. J. Heeger (2006) "New architecture for high-efficiency polymer photovoltaic cells using solution - based titanium oxide as an optical spacer," *Advanced Materials,* 18: 572–576.

[65] G. Yu, J. Gao, J. C. Hummelen, F. Wudl, and A, J. Heeger (1995) "Polymer photovoltaic cells: Enhanced efficiencies via a network of internal donor–acceptor heterojunctions," *Science,* 270:1789–1790.

[66] H. Hoppe, and N. H. Sariciftci (2006) "Morphology of polymer/fullerene bulk hetero-junction solar cells," *Journal of Material Chemistry,* 16: 48–58.

[67] W. Ma, C. Yang, X. Gong, K. Lee, and A. J. Heeger (2005). "Thermally stable, efficient polymer solar cells with nanoscale control of the interpenetrating network morphology," *Advanced Function Materials,* 15: 1617–1622.

[68] M. Reyes-Reyes, K. Kim, D. L. Carroll (2005) "High-efficiency photovoltaic devices based on annealedpoly(3-hexylthiophene and 1 -(3-methoxycarbonyl)-propyl-1-phenyl-(6,6) C61 blends," *Applied Physics Letters,* 87: 083506.

[69] R. H. Bube (1992) Photoelectronic Properties of Semiconductors; Cambridge University Press: Cambridge.

[70] C. J. Brabec, V. Dykonov, J. Parisi and N. S. Sariciftci (2003) "Organic Photovoltaics:concepts and realization," *Springer,* 60.

[71] O. Morton (2006) “Solar energy: A new dawning?: Silicon Valley sunrise,” *Nature*, 443: 19-22.

[72] S. E. Shaheen, R. Radspinner, N. Peyghambarian and G. E. Jabbour (2001) “Fabrication of bulk hetero-junction plastic solar cells by screen printing,” *Applied Physics Letters*, 79: 2996.

[73] W. L. Ma, C. Y. Yang, X. Gong, K. Lee, A. J. Heeger (2005). “Thermally stable, efficient polymer solar cells with nanoscale control of the interpenetrating network morphology,” *Advanced Function Materials*, 15:1622-1623.

[74] J. Van De Lagemaat, T. M. Barnes, G. Rumbles, S. E. Shaheen, T. J. Coutts, C. Weeks, I. Levitsky, J. Peltola, and P. Glatkowski (2006) “Organic solar cells with carbon nanotubes replacing In_2O_3: Sn as the transparent electrode,” *Applied Physics Letters*, 88(1): 23350.

[75] A. Heeger, N. S. Saricifti and E. B. Namdas (2010) “Semiconducting and metallic polymers,” Oxford Graduate Texts, Oxford University Press, New York.

[76] L. Zeng, C. W. Tang and S. H. Chen (2010) “Effects of active layer thickness and thermal annealing on polythiophene: Fullerene bulk hetero-junction photovoltaic devices,” *Applied Physics Letters*, 97: 5.

[77] R. S. Ohl (1941) “Light sensitive electric device,” US Patent 240266.

[78] M. A. Green, K. Emery, Y. Hishikawa, and W. Warta (2010) “Solar cell efficiency tables (version 35),” *Progress in Photovoltaics: Research and Applications*, 18:144.

[79] M. A. Green, K. Emery, Y. Hishikawa and W. Warta (2012) “Solar cell efficiency tables (Version 39),” *Progress in Photovoltaics: Research and Applications*, 20: 12

[80] M. A. Green, K. Emery, Y. Hishikawa, W. Warta, E. D. Dunlop (2013) “Solar cell efficiency tables (Version 42),” *Progress in Photovoltaics: Research and Applications*, 2: 827–837.

[81] M. A. Green, K. Emery, Y. Hishikawa, W. Warta, E. D. Dunlop (2014) “Solar cell efficiency tables (version 43),” *Progress in Photovoltaics: Research and Application,* 22:1–9.

[82] T. Erb, U. Zhokhavets, G. Gobsch, S. Raleva, B. Stuhn, P. Schilinsky, C. Waldauf and C.J. Brabec (2005) “Correlation between structural and optical properties of composite polymer/fullerene films for organic solar cells,” *Advanced Function Materials,* 15: 1193–1196.

[83] K. Kim, J. Liu, and D. L. Carroll (2006) “Thermal diffusion processes in bulk hetero-junction formation from poly-3-hexylthiophene/C60 single hetero-junction photovoltaics,” *Applied Physics Letters,* 88: 181911.

[84] N. S. Sariciftci and A. J. Hebger (1994) “Reversible, Metastable, Ultrafast Photoinduced Electron Transfer from Semiconducting Polymers to Buckministerfullerene and in the corresponding Donor/Acceptor Hetero-junctions,” *International Journal of Modern Physics B,* 08:237.

[85] C. W. Tang (1986) “Two layer organic photovoltaic cell,” *Applied Physics Letters,* 48(2): 183-185.

[86] Y. Zhao, Z. Xie, Y. Qu, Y. Geng and L. Wang (2007) “Solvent-vapor treatment induced performance enhancement of poly(3-hexylthiophene):methanofullerene bulk-heterojunction photovoltaic cells,” Applied Physics Letters, 90: 043504.

[87] M. Campoy-Quiles, M. Sims, P. G. Etchegoin, and D. D. C. Bradley (2006) “Thickness-dependent thermal transition temperatures in thin conjugated polymer films,” *Macromolecules,* 39: 7673–7680.

[88] H. Kim, W. W. So and S. J. Moon (2006) “Effect of thermal annealing on the performance of P3HT/PCBM polymer photovoltaic cells,” *Journal of Korean Physical Society,* 48: 441–445.

[89] H. J. Snaith, N. C. Greenham, and R. H. Friend (2004) “The origin of collected charge and open-circuit voltage in blended polyfluorene photovoltaic devices,” *Advanced Materials,* 16: 1640–1645.

[90] J. R. Xue, B. P. Rand, S. Uchida, and S. R. Forrest (2005) “Mixed donor–acceptor molecular hetero-junctions forphotovoltaic applications. II. Devices performance,” *Journal of Applied Physics Letters,* 98: 124903.

[91] V. Zhokhavets, T. Erb, G. Gobsch, M. Al-Ibrahim, and O. Ambacher (2006) “Relation between absorption and crystallinity of poly(3-hexylthiophene)/fullerene films for plastic solar cells,” *Chemical Physical Letters,* 418: 347–350.

[92] E. Klimov, W. Li, X. Yang, G. G. Hoffmann, J. Loos (2006) “Scanning near-field and confocal Raman microscopic investigation of P3HT:PCBM systems for solar cell applications,” *Macromolecules,* 39: 4493–4496.

[93] V. Zhokhavets, T. Erb, H. Hoppe, G. Gobsch, and N. S. Sariciftci (2006) “Effect of annealing of poly(3-hexylthiophene)/fullerene bulk hetero-junction composites on structural and optical properties,” *Thin Solid Films,* 496: 679–682.

[94] T. J. Savenije, J. E. Kroeze, X. Yang,and J. Loos (2005) “The effect of thermal treatment on the morphology and change carrier dynamics in a polythiophene-fullerene bulk hetero-junction,“ *Advanced Function Materials,* 15: 1262–1266.

[95] B. O'Regan and M. Grätzel (1991) “A low-cost, high-efficiency solar cell based on dye-sensitized colloidal TiO_2 films,” Nature, 353(6346): 737–740.

[96] M. Grätzel (2003) “Dye-sensitized solar cells,” *Journal of Photochemistry and Photobiology C: Photochemistry Reviews,* 4: 145–153.

[97] G. Kalonga, G. K. Chinyama, M. O. Munyati and M. Maaza (2013) “Characterization and optimization of poly (3-hexylthiophene-2, 5- diyl) (P3HT) and [6, 6] phenyl-C61 - butyric acid methyl ester (PCBM) blends for optical absorption,” 4(7): 93-102.